A high-resolution transient 3-dimensional hydrological model of an extensive undisturbed bog complex in West Siberia

W. Bleuten[1], E. Zarov[2], O. Schmitz[1]

[1]Department of Physical Geography, University of Utrecht, The Netherlands
[2]UNESCO Chair of Ugra State University, Khanty-Mansiysk, Russian Federation

SUMMARY

Data on the distributed dynamics of water table elevation (WTE) and on the variation of water discharge are needed for calculation of the carbon balances of entire mire complexes. Here we describe the development of a high-resolution transient hydrological model for the extensive boreal bog complex at Mukhrino in West Siberia (Asian Russia). The model, developed in PCRaster-MODFLOW, outputs spatially distributed WTE and daily water fluxes in 3D. It incorporates snowmelt dynamics and temporal freezing of the upper peat layer. During the period 2008−2016 snowmelt occurred during 2−4 weeks per year and accounted for 30 % of the total volume of water available for recharge and evapotranspiration. The calibrated hydraulic conductivity of the acrotelm was 0.6−1.2 cm s^{-1}. Model outputs indicated that the annual amplitude of WTE variation was 10−20 cm, in agreement with on-site measurements. Snowmelt raised the water table by 5–10 cm at the water divide and by 10–20 cm near the margin of the bog. In the ridge-hollow complex on the mire expanse, 91 % of all spring water fluxes discharged through the acrotelm in hollows, whereas the ridges retarded runoff. Based on modelled water fluxes and measurements of DOC we estimated that the organic carbon (DOC) export from the bog complex was 7.7 g m^{-2} y^{-1}.

KEY WORDS: DOC export, evapotranspiration, hydraulic conductivity, MODFLOW, snowmelt, water table

INTRODUCTION

Boreal mires (bogs and fens) are important sinks and sources of atmospheric carbon (C) (Silvola *et al.* 1996), which makes mires relevant for climate change feedback (Turunen *et al.* 2001, Belyea & Malmer 2004). Estimates of carbon gas exchange between the mire surface and the atmosphere are commonly based on point measurements from eddy covariance towers (Baldocchi *et al.* 2001, Alekseychik *et al.* 2017) or flux chambers (Christensen *et al.* 1995, Kutzbach *et al.* 2004, Dyukarev *et al.* 2019). Eddy covariance measurements represent fluxes from a homogeneous footprint area, whose size and location varies with meteorological conditions (wind) (Kormann & Meixner 2001). Bog complexes are not homogeneous in surface roughness, which complicates extrapolation by this method. When applying chambers, simultaneous measurements at a great number of sites are needed to effectively assess C gas exchange across a mire area.

One of the key environmental factors influencing the intensity of C fluxes between mires and the atmosphere is the level of the water table relative to the mire surface, or water table depth (WTD) (Moore *et al.* 1998, Belyea & Clymo 2001, Hilbert *et al.* 2003, Yurova *et al.* 2007, Mezbahuddin *et al.* 2016, Wu *et al.* 2016). Therefore, calculation of the carbon balance of an entire bog complex can be facilitated by an area-wide knowledge of the pattern and dynamics of WTD.

Quantification of the dynamics of water discharge from bog complexes is also important for calculating the carbon balance, because part of the organic carbon accumulated by primary production is decomposed, released and dissolved in superficial bog water and subsequently exported to fluvial systems (Moore *et al.* 1998, Fraser *et al.* 2001, Strack *et al.* 2008, Waddington *et al.* 2009, Broder & Biester 2015, Leach *et al.* 2016). Export of dissolved organic carbon (DOC) from natural peatlands has been correlated with discharge (Dinsmore *et al.* 2013, Olefeldt *et al.* 2013) and the occurrence of snowmelt (Fraser *et al.* 2001, Campeau *et al.* 2017).

Observing runoff from mire complexes is difficult because part of the water leaving a bog flows over and through the acrotelm (Ivanov 1957, Ingram 1978, Holden & Burt 2003), crosses lagg fens at the perimeter, and enters diffusely draining streams and rivers. It is expected that bog water passing through the catotelm (Ivanov 1957, Ingram 1978) is of minor importance because hydraulic conductivity decreases downwards in peat layers (Ivanov 1957, Fraser *et al.* 2001). On the other hand, the calculation of both

WTD and water export is impeded by spatial variation in the amplitude of 'mire-breathing' (Roulet 1991, Kellner & Halldin 2002, Price 2003, Howie & Hebda 2018).

Because the surface level of a mire system (macrotope or mesotope) varies between mire types such as raised bog and fen, and at smaller (microtope) scale due to the presence of hummocks, ridges and hollows (Laitinen *et al*. 2007, Eppinga *et al.* 2008), both WTD and water discharge are spatially variable (Shi *et al.* 2015). They also change seasonally and from year to year due to temporal variations in snowmelt, rainfall and evapotranspiration (Wu *et al.* 2016).

Hydrological models are useful aids to understanding and quantifying the processes operating in a peatland (Whitfield *et al.* 2009) and can produce data on WTD and water discharge. However, numerical models of peatland systems are often oversimplified or misrepresent the complex structure of typical mire systems by omitting the effects of snowmelt, ground frost and (mire type dependent) patterns of hydraulic properties, peat-surface adjustments and evapotranspiration. For instance, Ivanov (1981) conducted extensive depthwise measurements of saturated hydraulic conductivity (K_{sat}) in the peat layers of undisturbed bogs and used these data for one-dimensional (1D) calculation of flow paths, but did not explicitly calculate discharge. Other 1D approaches, for example by Weiss *et al.* (2006), Dimitrov *et al.* (2010), Edom *et al.* (2010), Frolking *et al.* (2010), Cresto Aleina *et al.* (2015), Shi *et al.* (2015), Chaudhary *et al.* (2017) and Mackin *et al.* (2017) are not applicable to the prediction of WTD patterns without assumptions about percolation losses, horizontal flow variations and overland flow. The 2D (quasi 3D) model described by Baird *et al.* (2012) cannot model vertical flow well and therefore offers limited possibilities for predicting water flow in different mire types (van der Schaaf 1999, van der Ploeg 2012). The model by Reeve *et al.* (2001) is 2D (vertical cross sections), which means it cannot produce a spatial pattern of WTD. The 2D steady state modelling by Lapen *et al.* (2005) considers a blanket bog, which is dissimilar from most other northern mire types. Steady state models in 3D have been developed by Reeve *et al.* (2001) and Borren & Bleuten (2006), using cell lengths of 2.5 km and 200 m, respectively. With such cell dimensions it is not possible to calculate WTD differences between mire types or to take into account the effect of damming by ridges in ridge-hollow complexes as described by van der Schaaf (1999), Eppinga *et al.* (2008) and van der Ploeg (2012). None of the modelling attempts mentioned above considered all of the critical hydrological processes in a natural bog at a scale compatible with mire patterning and, therefore, none predicted well the dynamics and patterns of WTD and water discharge.

The objective of this study was to develop a hydrological model of an undisturbed bog complex to enable prediction of the fine-scale pattern and dynamics of water table depth and water fluxes, based on precipitation, snow and evapotranspiration data. Sub-targets were to quantify: (i) the distribution of peak water discharge and (ii) the dynamics of DOC export.

METHODS

Study site

The study site is located next to the Mukhrino International Field Research Station, 21 km south-west of Khanty-Mansiysk town (Figure 1) within the 'Middle Taiga Sub-Zone' (Gvozdetskii *et al.* 1973, Kosykh *et al.* 2008). This mire (approximately 75 km^2) developed within a depression in the upper terrace of the Irtysh River between the Mukhrino River in the east and the Bolshaya River in the west. The eastern border of the mire massif is defined by a wavy scarp rising 2–6 m above the floodplain. The heads of tributary brooks of the Mukhrino River penetrate up to 500 m into the mire, exposing the peat layers and the upper part of the silty river terrace sediments. The peat layers near the scarp have been drained by this natural process, and deep cracks are forming. A true waterfall created on a bog brook (a small stream emerging from the peatland) at the rapidly retreating (at 0.1 m y^{-1}) peat edge provides a unique opportunity for measurement of mire water discharge.

The mire is a bog complex (Lapen *et al.* 2005) consisting of large areas of 'ryam' (an indigenous name) with shallow depressions (0.1–2 km^2) and tall hummocks, mainly near the margins, and a central patterned area (Figure 2). The ridge-hollow patterning in the centre of the complex consists of elongated ridges (width 5–20 m) and oval hollows (10 × 100 m). Parts of the hollows contain shallow pools with peat floors. In some places the pools form oligotrophic ladder fens (McCarter & Price 2017). There are also several deep primary lakes (with mineral floors) within the bog complex. Tall mixed forest grows on a few mineral islands within the mire and on the mineral soils at its margins.

Climate

The climate in the central part of West Siberia is continental (average annual temperature -2.1 °C)

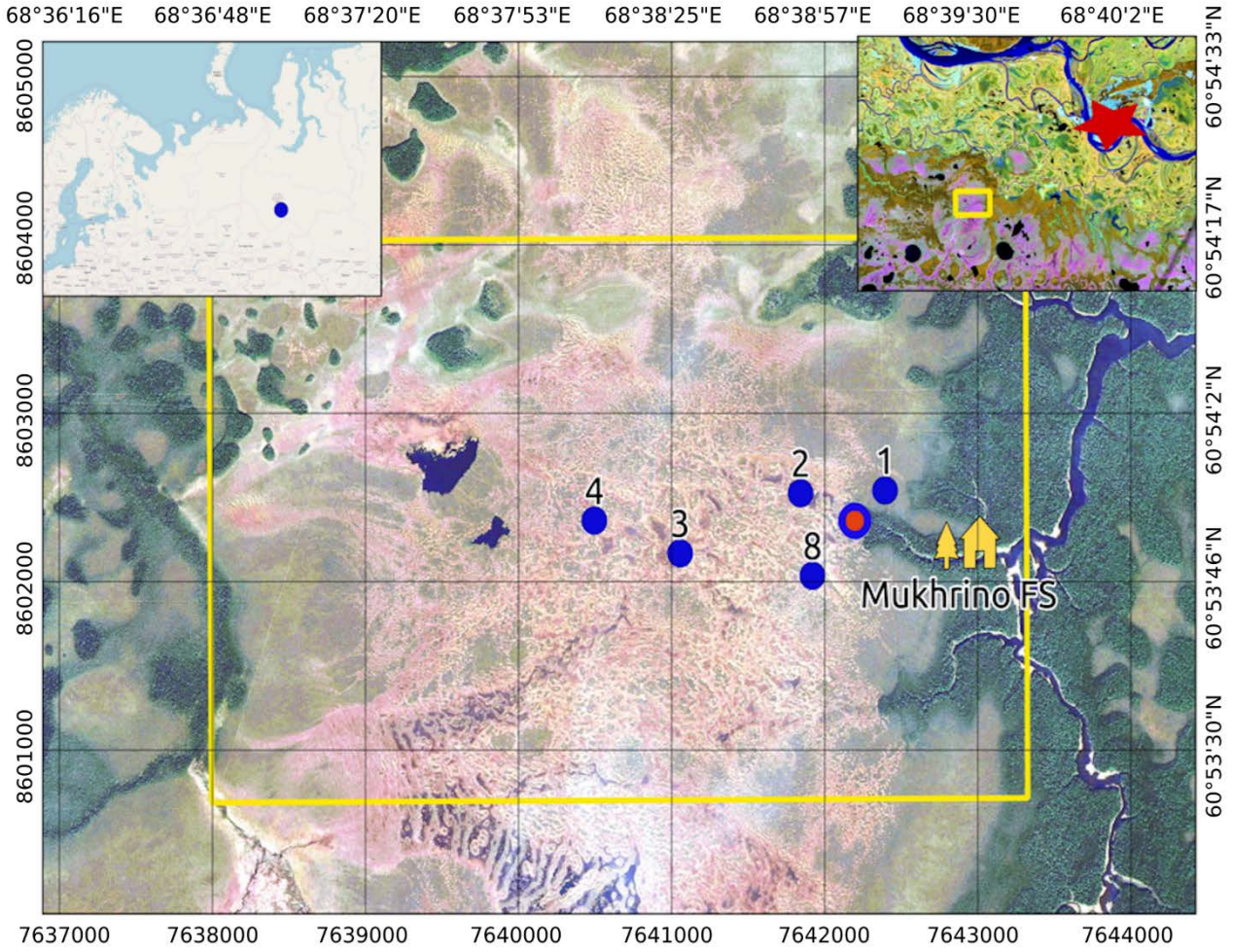

Figure 1. Location map of part of the Mukhrino bog complex based on Quickbird and LandSat-5 satellite images. Mukhrino FS = Mukhrino International Field Research Station (60.89 °N, 68.70 °E); green = mixed forest; purple = mire; yellow box = model area; blue filled circles = water level tubes; red filled circle = weir in bog brook. Upper right (inset): map of Khanty-Mansiysk region; light green and yellow = floodplains of the Ob and Irtysh Rivers; blue = rivers; brown-green = mixed forest; purple = mire; large red asterisk = Khanty-Mansyisk town. Labels around the edges of the image are in metres (UTM).

with high summer temperatures (July mean 17.9 °C) and low winter temperatures (January mean -20.7 °C) (Kosykh *et al.* 2008). According to data from Meteorological Station Khanty-Mansiysk (MS-XM), located about 25 km north-east of the study area, average precipitation for the period 2008–2016 was 744 mm y^{-1} (2.04 mm d^{-1}) with 33 % as snow (RP5.RU 2017). The 2008–2016 mean maximum snow depth was 0.6 m. There is no permafrost in the study area.

Land unit types

A map of the land unit types (LUTs) present in the 16.9 km^2 model area (Figure 1) was developed by supervised classification of a high resolution (2.44 m) Quickbird satellite image and ground truthing of 25 key areas. Seven LUTs were identified, namely: river (and floodplain), (primary) lake, pool, hollow, ridge, ryam and (mixed) forest. The resulting map is shown in Figure 2, and Table 1 gives concise descriptions of the LUTs.

Digital elevation model (DEM)

A digital elevation model (DEM) of the area was prepared from an extensive levelling survey using differential GPS (dGPS). Because of the poor accessibility of the bog complex, the dGPS measurements were taken over several years. Fieldwork was carried out mostly during winter in order to avoid inconsistencies arising from instability of the unfrozen mire surface. Thus, in practice, we levelled the frozen top of the peatland.

Two receivers (Maxor-GGDT Javad; horizontal accuracy 3 mm, vertical accuracy 5 mm) were used

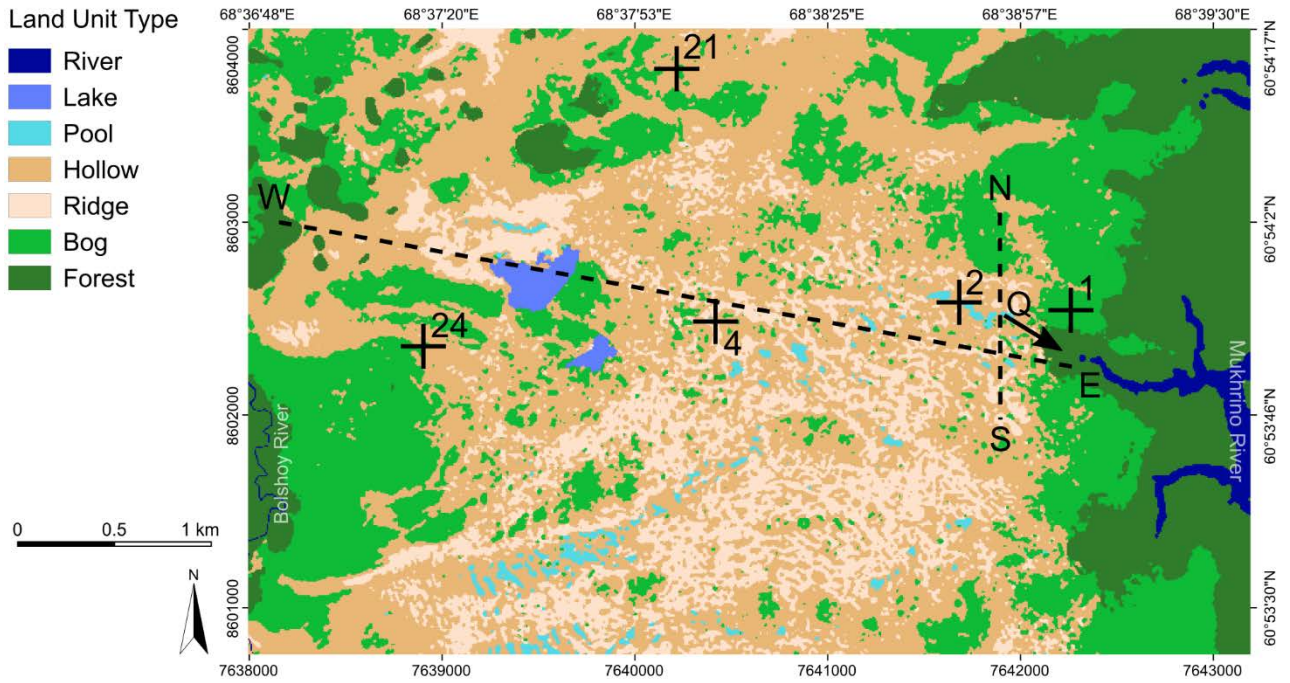

Figure 2. Map of land unit types (LUTs) of the Mukhrino study area. River = river channel and floodplain; lake = deep primary lake; pool = open water in hollows; hollow = hollows in ridge-hollow complex and sedge - *Sphagnum* lawns; ridge = ridges of ridge-hollow complex; ryam = bog with trees; forest = mixed forest on mineral soil; Q = outlet of bog brook. Crosses indicate the locations of the head graphs shown in Figure 9; and broken lines the locations of the cross sections shown in Figure 10 (W–E) and Figure 11 (N–S).

Table 1. General descriptions of the classified land unit types (LUTs).

Land Unit Type		**Description**
1	River	Open water and floodplain vegetation of sedges and grasses.
2	Lake	Open water, mineral subaquatic soil.
3	Pool	Areas of shallow open water with peaty floors occurring in hollows of ridge-hollow microtope.
4	Hollow (of ridge-hollow complex)	Treeless moss-sedge (*Sphagnum balticum, Sphagnum jensenii, Sphagnum majus, Carex limosa, Scheuchzeria palustris, Rhynchospora alba, Oxycoccus* ssp., *Drosera* spp.) plant community on peat soil, water table depth 3–15 cm, mostly quagmires. Top of mosses usually 30–50 cm below ridge (Type 5) level.
5	Ridge (of ridge-hollow complex)	Patches with ericaceous dwarf shrubs (*Ledum palustre, Chamaedaphne calyculata, Andromeda polifolia*), *Sphagnum* mosses (*Sphagnum fuscum, Sphagnum angustifolium*) and pine (*Pinus sylvestris*) on peat soil, 3–20 m wide and up to ~200 m long), linearly extended perpendicular to direction of water flow, water table depth 15–30 cm.
6	Ryam (bog with high hummocks)	Extensive areas of hummock-hollow microtope with ericaceous dwarf shrubs (*Ledum palustre, Chamaedaphne calyculata, Andromeda polifolia*), *Sphagnum* mosses (*Sphagnum fuscum, Sphagnum angustifolium*) and pine (*Pinus sylvestris*) on peat soil, water table depth 15–50 cm.
7	Forest	Tall aspen and fir mixed forest with ericaceous herb layer *(Vaccinium myrtillus, Vaccínium uliginosum, Vaccinium vitis-idaea*) on organic-mineral soil, peat not present.

in kinematic regime. A base station was located at a fixed position for the entire levelling session (533 occupation points). Surface elevation (altitude) measurements were recorded by 3 replications of 3 minutes each. Median elevation was calculated for each point by post processing with Pinnacle software (Javad Ensemble). The table of results was converted to shapefile format and loaded into the SAGA geo-information system, and interpolation was performed by the inverse weighted distance (IDW) method.

The DEM (Figure 3) was constructed as follows. In ridge-hollow complexes we took the level of the top surface of the moss carpet in hollows, as an approximation to the top of the catotelm (the ridges protruded 0.3–0.5 m above the hollows). In ryam the average level of the top surface of moss on hummocks and in lows between hummocks was used. The average water levels (as water table elevation, WTE) in lakes and pools were assumed to correspond to the hollow levels. The depth of the riverbed below the river banks (0.5 m) was measured manually.

Peat layers

An intensive peat coring programme was conducted to investigate the vertical sequence of fossil plant remains (species abundance). An east–west cross section is presented in Figure 4. The bog complex has a convex profile overall, the central part rising about 1.2 m above the margin. Average peat depth is 3.3 m. The central part of the cross section shows the presence of an ancient valley incised into the Pleistocene mineral terrace. The valley first filled up with gyttja deposits then, under the influence of rising water table, the area changed into a swamp where thin layers of eutrophic wood peat and horsetail/fern peat accumulated, followed by alternating layers of brown moss-sedge peat and *Sphagnum* moss peat. The most abundant peat types are *Sphagnum fuscum* peat (35.33 %), complex peat (14.5 %) and hollow peat (6.8 %) (Zarov 2013).

Dissolved organic carbon (DOC) measurements

A 0.2 m deep, 60 m long interception channel was excavated to conduct water draining from the mire catchment to a V-notch weir at the waterfall in the bog brook at the eastern side of the site (Figure 1). Discharge was calculated from pressure transducer (Mini-Diver D1501, accuracy ± 5 mm H_2O) data and a standard Q-h equation calibrated for this weir (Bleuten & Filippov 2008).

For determination of DOC export, single water samples (40 cm^3) were collected monthly from the beginning of snowmelt (May) until the establishment of stable snow cover (October) each year, throughout the period 2010–2015. All samples were passed through 0.45 µm membrane filter (Whatman GD/X), cooled and transported to the Yugra State University laboratory. DOC concentrations were measured by Tuirin's method for determination of soil organic carbon, modified to use a spectrophotometer (GOST

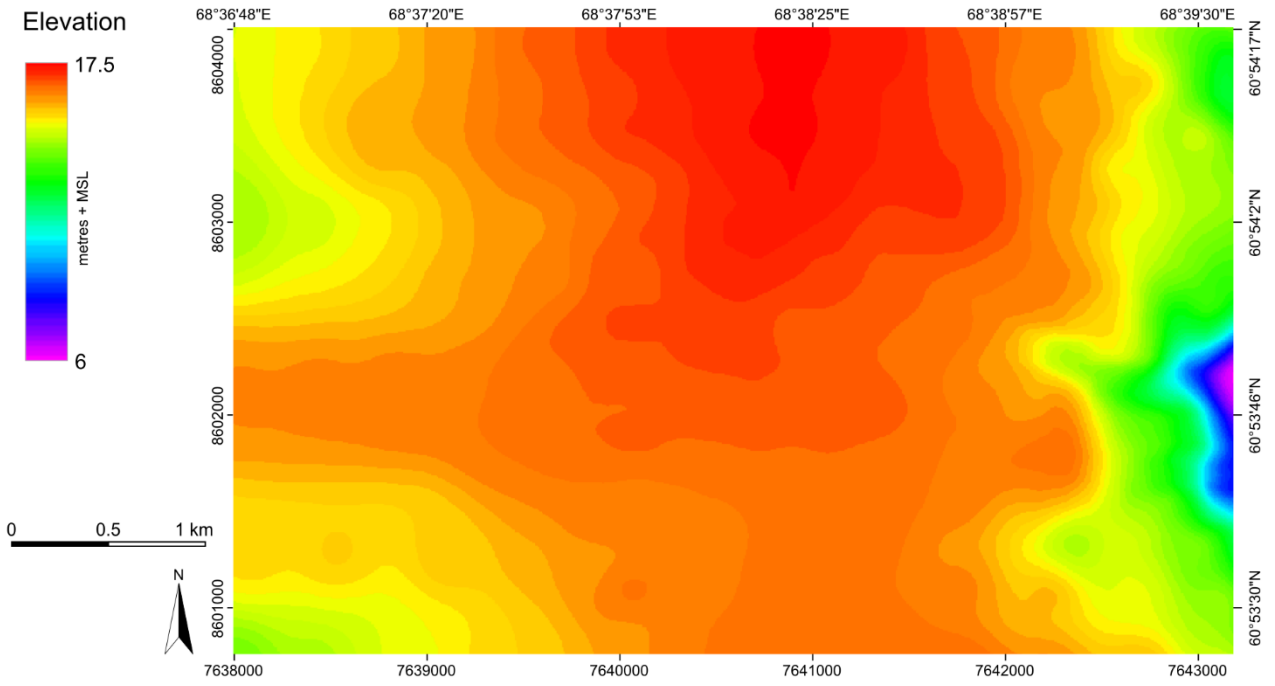

Figure 3. Digital Elevation Model (DEM) of the study area, which covers part of the extensive Mukhrino Bog complex (see Figure 8 for location within the peatland). Constructed from dGPS data collected on-site.

1991). More information about the method is provided in the Appendix.

Modelling hydrology

During field studies since 2002 it was observed that low winter temperatures caused the top layers of lakes and peatland to freeze to a depth of 0.5 m. In spring (April–May), the snowpack usually melted within 1–2 weeks and the runoff water was retained in hollows and pools until the intervening ridges became free of snow and ice. The maximum flow velocities observed for runoff in water tracks was 0.05 m s^{-1}. In dry summer periods the rate of water discharge was reduced due to high evapotranspiration.

A model was built with PCRaster-MODFLOW (Harbaugh *et al*. 2000, Schmitz *et al*. 2009) to analyse overland flow, subsurface flow and groundwater flow within a selected area of the Mukhrino bog complex. The model output gives WTE (head) distributed over the model area and cell-by-cell water fluxes in the X, Y and Z directions under steady state or transient conditions (see Appendix for more information about PCRaster-MODFLOW). We first

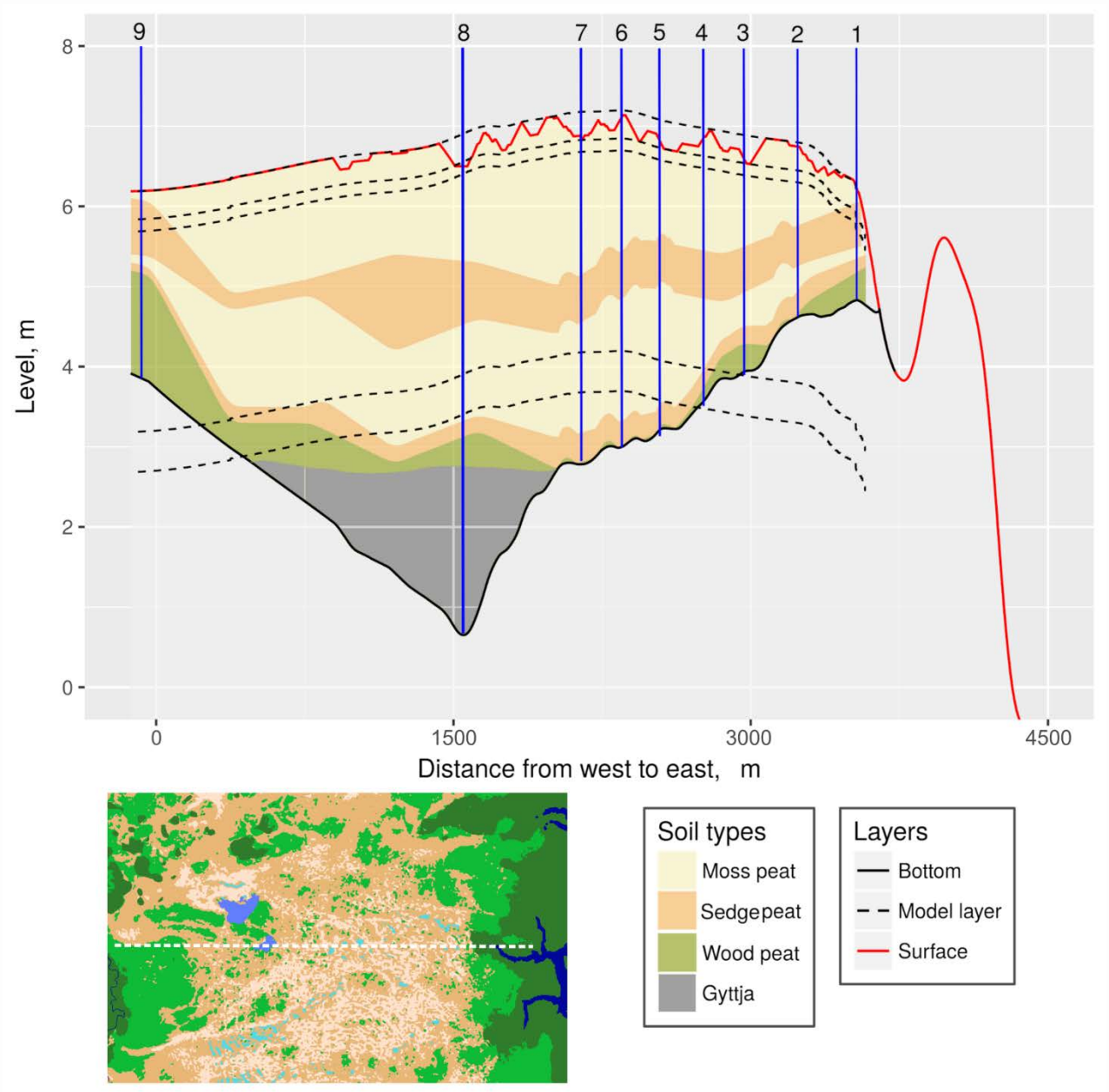

Figure 4. Cross section through the study area showing the composition of peat layers derived by coring (vertical blue lines indicate locations of cores) and the arrangement of model layers. The location of the profile is shown by the white dotted line on the inset satellite image.

built a 3D steady state model to calculate parameters for the peat layers, then a 3D transient model was developed using the layer data of the steady state model. We postulated that flow velocities would be low due to resistance by vegetation and, therefore, that Darcy's law was applicable (Hemond & Goldman 1985).

Because it was our objective to analyse water fluxes and WTE variations at fine scale, the resolution of the model should be sufficient to calculate the effects on water flow of the ridges in ridge-hollow microtopes (we expected hydraulic conductivity to be lower in ridges than in hollows; see Table 3). The ridges are 5–20 m wide, making a resolution of 5 m preferable. However, such resolution was not feasible in terms of runtime and computer memory requirements, given the size of the area to be modelled (16.9 km^2). Therefore, we chose a cell size of 7 m × 7 m. The model size was 464 × 743 cells in 5 layers (total 1,723,760 cells). We selected a time step length of one day in order to enable the modelling of peak discharge events.

The model area was bounded to the west by the valley of the Bolshaya River and to the east by tributaries of the Mukhrino River (Figure 2). At both of these model boundaries, WTE (drain elevation) was assumed to be constant at 2 m below the annual mean WTE on the bog. Along these boundaries we placed drains inside the acrotelm layer to simulate diffuse radial water flow as described by Ivanov (1957). The northern and southern boundaries of the model area were assumed to coincide with water flow paths (i.e. no groundwater flow across these boundaries, but WTE may vary).

Calculation of recharge

The volume of water (recharge) which reaches the phreatic surface in peat or open water depends on the precipitation input (rainfall plus snowmelt water) minus losses by evapotranspiration.

Precipitation data (rain and snow per day, both presented in mm) are available on the internet (RP5.RU 2017) from MS-XM. The range of snowpack depth was 40–110 cm. We assumed zero groundwater recharge during frost periods (when the top 0.5 m of peat was frozen). To estimate the water volume produced by snowmelt, the water content of the snowpack available for melting and the melting rate should be known. We computed snowpack depth, ablation and snowmelt using a degree-day model calibrated with the daily snow depth data provided by MS-XM for the period 01 Jan 2008 to 01 May 2008 (see Appendix).

Actual evapotranspiration (E_a) was calculated from the reference evapotranspiration (E_{ref}) using a land unit type dependent reduction factor f (Feddes 1987), as:

$$E_a = f_i \times E_{ref} \quad [1]$$

where f_i is the reduction factor by land unit type. For E_{ref} the empirical formula of Makkink (Makkink 1957, Moors 2008) was applied, because the data published by MS-XM do not include reference evapotranspiration. The more commonly applied Penman-Monteith method (Allen *et al.* 1998) for E_{ref} calculation could not be used because the necessary variables were not available. The Makkink formula requires only temperature and solar radiation as variables. E_{ref} (m d^{-1}) was calculated for days with $T_t > 0$ as:

$$E_{ref} = 0.65 \times \frac{s}{(s+0.66)} \times \frac{R}{245} \quad [2]$$

where s is the slope of the saturation vapour pressure - temperature curve and R is solar radiation (J m^{-2} d^{-1}); calculated as follows:

$$s = 0.4654 \times EXP\left(\frac{0.0544 \times T_t}{10}\right) \quad [3]$$

$$R_t = \frac{24.6}{Lhd} \times SE_t \times CR_t \quad [4]$$

where T is mean day temperature (°C), t is time step (days), Lhd is daylight hours, SE is solar elevation (calculated from latitude), and CR is reduction by cloud coverage. Cloud cover data were obtained from MS-XM.

The evapotranspiration reduction factor (f_i) for each land unit type (Equation 1) was iteratively approached (to achieve best agreement with actual measurements of WTE) by changing specific yield and percolation in a 1D model which calculates daily WTE (head; H_t) using precipitation (P_t) and evapotranspiration data:

$$H_t = H_{t-1} + \frac{P_t - (f_i \times E_{ref(t)})}{SY} - Z \quad [5]$$

where SY is specific yield and Z is mean daily loss by percolation.

Actual WTE was recorded with five pressure transducers (mini-Diver D1501) placed in slotted 2.5 cm diameter polypropylene tubes at the locations shown in Figure 1. Each tube (up to 4 m long, with 0.5 m long saw slots at depths of 1.5–3.5 m below the surface) was installed in a separate borehole prepared with a Russian peat corer, and anchored in the mineral subsoil. Logger 1 was located in ryam about 120 m from the eastern margin of the bog. Logger 2

was located at the edge of a hollow about 380 m from the eastern bog margin. Loggers 3 and 4 were located in hollows close to pools in the centre of the bog, near the water divide. Logger 8 was placed in a ridge about 300 m from the bog margin. Because the hydraulic conductivity of deeper (> 1 m below surface) peat layers is very small at all of these points, water loss by vertical percolation (Z-percolation) should be low. Unfortunately, four of the WTE records could not be expressed as complete time series due to insufficient control data, gaps and programming mistakes. However, parts of the records of relative heads from all five pressure transducers could be used for calibration of evapotranspiration factors.

Recharge per land unit type was calculated using the following equation:

$$Rech_{t,i} = Sm_t + P_t - Ea_{t,i} \quad [6]$$

where *Sm* is snowmelt, *P* is rainfall, *Ea* is actual evapotranspiration from Equation 1 and *i* refers to the LUT. Mean annual recharge for the steady state model was calculated using data for the 8-year period 2008–2016.

Definition of model layers

The elevations of the tops and bottoms of the five model layers (Figure 5) were calculated in PCRaster, based on the DEM (Table 3). The presence of a valley in the bog layer (Figure 4) was not included in the model scheme because we had insufficient information about the disposition (orientation, depth) of the valley within the model area.

Rivers and drains

The Mukhrino River (MR) and the Bolshaya River (BR) were modelled as DRAINS. The advantage of the DRAINS module in MODFLOW is that WTE may vary and the drain may eventually become dry. Brooks in bogs may dry up at the end of the summer season, which is an argument in favour of the use of DRAINS. BR is 5–10 m wide and incised to a depth of approximately 0.5 m. In the model we used a line of drains each 1 cell wide. MR runs through an open floodplain and its WTE is affected by seasonal WTE changes in the (major) Irtysh River to the east. From June until the end of July the floodplain of MR is submerged. In the model we placed drains across the whole of the floodplain (LUT 'River' in Figure 2).

Layer hydraulic conductivity and drain conductance

Hydraulic conductivity (*K*) of the model layers and drain conductance (Dc) were determined by iterations of the steady state model. Except for open water and air layers we assumed that the vertical hydraulic conductivity was half of the horizontal conductivity (Table 3). The averaged difference between WTE calculated by a model run and the

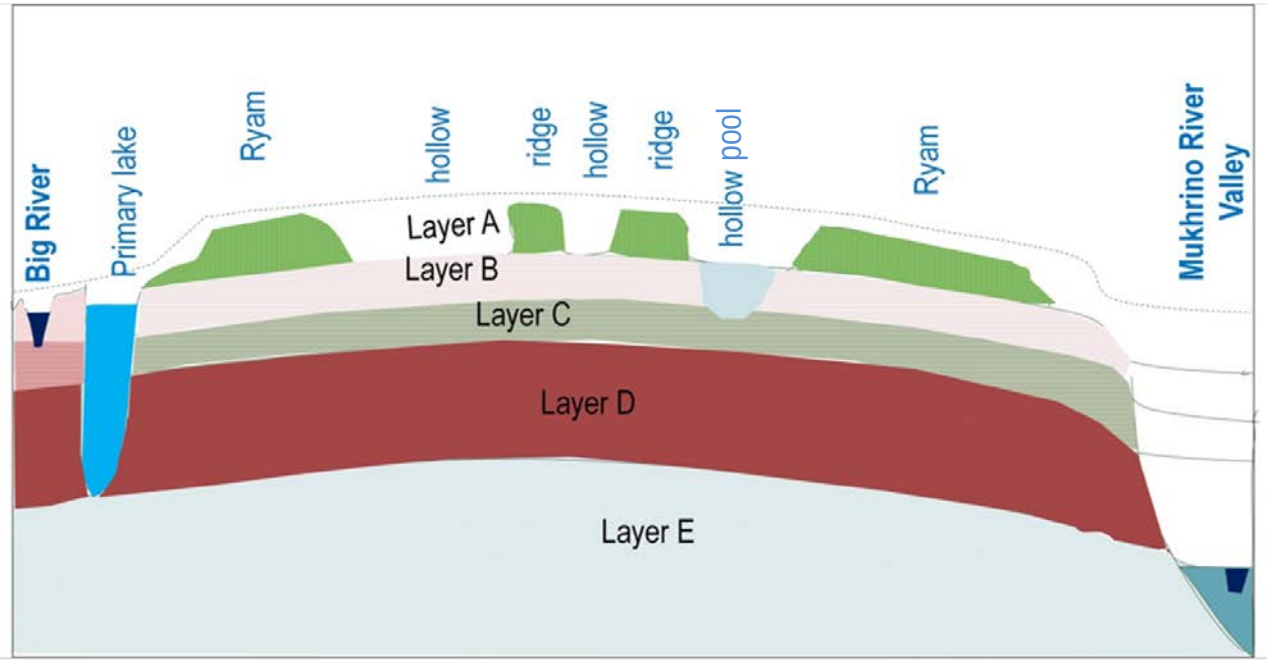

Figure 5. Schematic section across the model area showing the layers and rivers used for modelling. Layer A represents the acrotelm of ridge and ryam LUTs; Layers B, C and D are (catotelm) peat layers; and Layer E is the mineral subsoil.

DEM elevation in a central part of the model area should not exceed 0.03 m, which is comparable to observations in the area. Iterations were only accepted when the discrepancy of the water balance (MODFLOW output) was between -1 % and +1 %.

To simulate open water flow across the surfaces of hollows we used an "air" top layer (Figure 5) with $K = 1.16$ m s^{-1} . The same K value was used for open water in lakes and pools. In ryam and ridge parts of Layer A (acrotelm) K was set two orders of magnitude lower, at 1.16×10^{-2} m s^{-1}.

Transient modelling

For dynamic modelling a recharge input file (see the sub-section on "*Calculation of recharge*" above) with daily records (2008–2016) by LUT was used. During the winter period (01 December to 01 March) recharge was set to zero and Layer B (upper catotelm) K to 10^{-5} m d^{-1} (1.16×10^{-8} cm s^{-1}), supposing no downward water flow. We observed that the ice layer diminishes gradually in spring and it can be the end of June (sometimes even July) before all ice disappears. Therefore, in the transient model frozen conditions were assumed to persist from 01 December to 01 June.

For transient modelling, specific yield (*SY*) is required for all model layers which may become partially unsaturated. For the air top layer and open water, $SY = 1$ by definition. Other *SY* values (Table 2) were based on 1D modelling (Equation 5). Comparable *SY* values were found by Edom *et al.* (2010). To avoid the eventuality of cells falling dry permanently, we needed to use a 'rewetting' option (Doherty 2001; see Appendix).

RESULTS

Recharge

The snowpack sub-model produced very good results for the period 2009–2012. Results for the period 2012–2016 were less satisfactory (see Appendix 3). The results obtained using the snow model, averaged over eight years, were (in mm y^{-1}; ± standard deviation, SD): sublimation = 70 ± 10, snowmelt: 226 ± 90, and rainfall: 504 ± 98. Snowmelt occurred over a period of 2–4 weeks. The (8-year) average reference evapotranspiration calculated with Equation 2 was 262 (SD 32) mm y^{-1}. The LUT dependent evapotranspiration reduction factors, estimated with Equation 5, ranged from 0.9 to 1.2 (Table 2). An example of the WTE change modelled with a calibrated evapotranspiration value is presented in Figure 6.

Based on the 1D model (Equation 5) and the values from Table 2, the evapotranspiration reduction factors were set at: 0.9 for open water (river/ floodplain, lakes, pools); 1.0 for hollows; 1.1 for ridges and ryam; and 0.8 for forest. Recharge was calculated as the sum of snowmelt and rainfall minus LUT-dependent evapotranspiration. Figure 7 shows the pattern of mean recharge by LUT over the model area.

Modelled water table elevation (WTE)

Using the values of K and Dc presented in Table 3, the average deviation from the DEM of heads (WTE) calculated by the steady state model was 0.025 m with a water balance discrepancy of -0.2 % (Figure 8). This means that the water table is close to the top of the acrotelm. Calculated WTE was 0.1 m

Table 2. Calibrated evapotranspiration reduction factors (*f*), specific yield and Z-percolation values.

Logger	Surface type	*f*	Specific yield	Z-percolation mm d^{-1} (m s^{-1})
1	Ryam	1.2	0.3	0.03 ($3.47\ 10^{-7}$)
2	Hollow sedge lawn	1.1	0.8	0.05 ($5.79\ 10^{-7}$)
3	Hollow sedge lawn / pool *	0.9	1.0	0.0
4	Hollow sedge lawn / pool *	0.9	1.0	0.0
8	Ridge - ryam	1.2	0.6	0.0
-	Forest **	0.8		
-	Open water ***	0.95		

* water level recorded at the edge of a hollow-pool
** estimate
*** Bleuten & Bierkens 2015

below DEM at the northern part of the water divide and the north-east and west margins of the model area; and 0.2 m above DEM in the central and south-eastern parts of the model area.

For most of the model area, WTE (hydraulic head) calculated with the dynamic model varied by only a few decimetres. Five points (Figure 2) have been selected to illustrate the dynamics of WTE across the whole area (Figure 9). The smallest head variation was at the N–S water divide (Head 04 and Head 21 in Figure 9). In the northern part of the water divide (Head 21) WTE calculated by the steady state model was usually just below the DEM (= top of Layer B). Modelled heads at other points (except Point 01) varied from just above to slightly below the DEM. Hydraulic heads increased in response to snowmelt, by 5–10 cm at the water divide and by 10–20 cm near the margin of the bog (Head 02). Secondary head

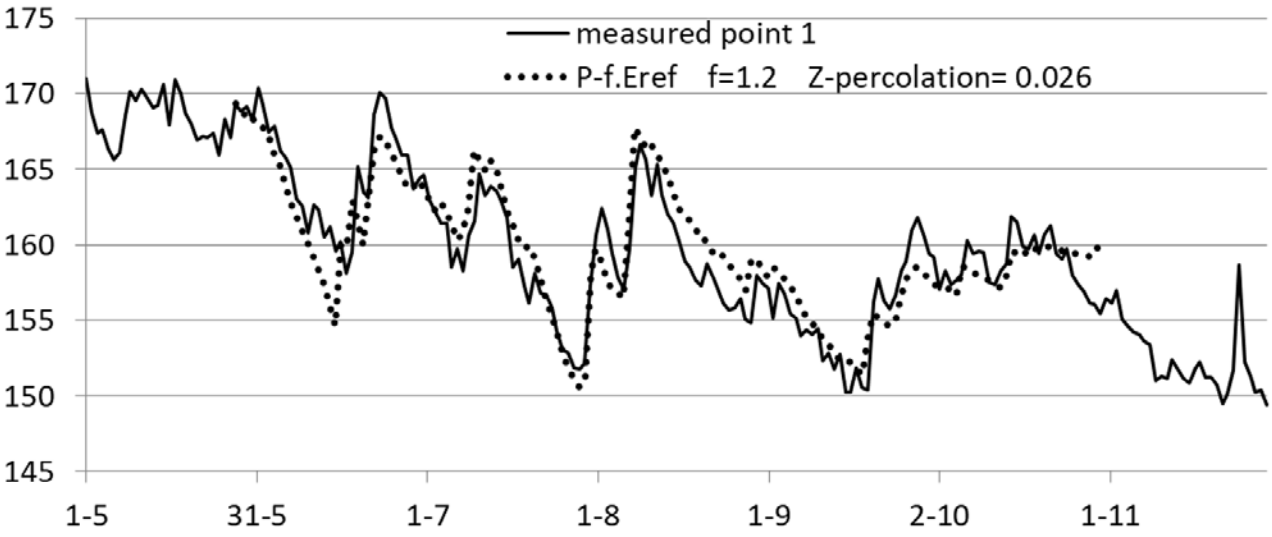

Figure 6. Calibration of the evapotranspiration reduction factor using water level data recorded in 2009 at the 'ryam' site (Point 1 in Figure 1). Model: $dH = P - (f \times E_{ref}) - Z_{percolation}$ (Equation 5). Y-value: relative water level in m.

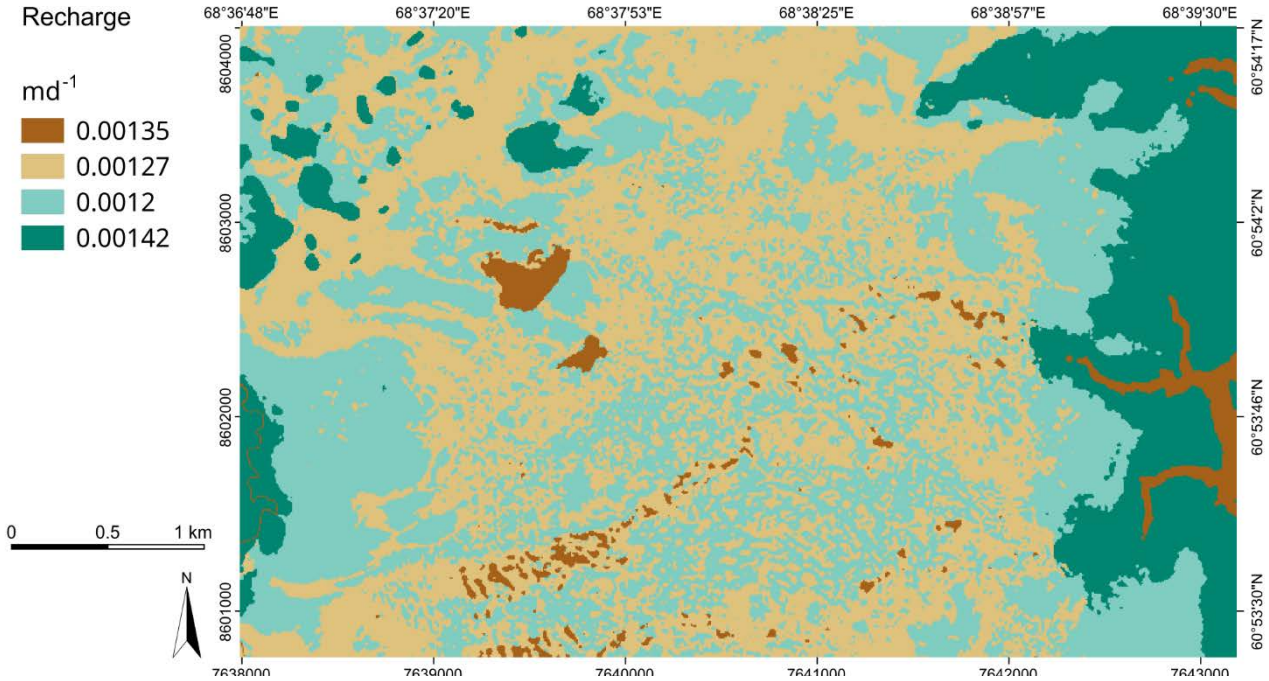

Figure 7. Average recharge by land unit type, in m d^{-1} (m s^{-1}). River floodplain, lake and pool: 0.00135 (1.56×10^{-8}); hollow: 0.00127 (1.47×10^{-8}); ridge and ryam: 0.0012 (1.39×10^{-8}); forest: 0.00142 (1.64×10^{-8}).

peaks occurred due to summer rainstorms. Variation in Head 01 was much larger than at the other four points because the location was within the marginal zone where the peat has drained naturally. In the western part of the model area (Head 24) the bog is not drained and head variation was small compared to the eastern part. The generally lower heads in the year 2014 can be explained by relatively low recharge. The range of modelled head fluctuations corresponds to observed variation in WTE at the three points chosen to coincide with pressure transducer locations (Head 01, 02, 04). Recorded WTE at the bog margin had the same range and fluctuations as modelled 'Head 01' (Figure 9).

Table 3. Input variables of the SS-Mukhrino model: elevation of model layers in m relative to DEM, horizontal conductivity (K_h cm s^{-1}), vertical conductivity (K_v cm s^{-1}), specific yield and drain conductance (Dc m^2 s^{-1}). Bottom of layer E = Mean Sea Level (MSL) = 0 m.

Layer	**elevation m**
top A	DEM + 0.5
top B	DEM
top C	DEM - 0.3
top D	DEM - 1.0
top E	DEM - 3.5

	horizontal conductivity cm s^{-1}						
	river	**lake**	**pool**	**hollow**	**ridge**	**ryam**	**forest**
K_h A	115.741	115.741	115.741	115.741	1.157	0.579	0.024
K_h B *	5.787	115.741	115.741	1.157	0.579	0.232	0.024
K_h C	5.787	115.741	1.157	0.116	0.116	0.116	0.024
K_h D	5.787	5.787	0.002	0.002	0.002	0.002	0.024
K_h E	0.023	0.023	0.023	0.023	0.023	0.023	0.023
	vertical conductivity cm s^{-1}						
K_v A	115.741	115.741	115.741	115.741	1.157	0.579	0.024
K_v B *	5.787	115.741	115.741	0.579	0.289	0.116	0.024
K_v C	5.787	115.741	1.157	0.058	0.058	0.058	0.024
K_v D	5.787	5.787	0.001	0.001	0.001	0.001	0.024
K_v E	0.023	0.023	0.023	0.023	0.023	0.023	0.023
	specific yield						
A	1.0	1.0	1.0	1.0	0.9	0.9	1.0
B	0.9	1.0	1.0	0.9	0.7	0.7	0.9
C	0.3	1.0	0.9	0.7	0.5	0.5	0.3
D	0.3	1.0	0.2	0.1	0.1	0.1	0.3
E	0.3	1.0	0.5	0.5	0.5	0.5	0.3

* frozen from 01 Dec to 01 Jun: $K = 1.16\ 10^{-8}$ cm s^{-1}

DRAINS	**elevation m**	**conductance m^2 s^{-1}**
Mukhrino River	DEM - 3.0 or 11.0 m above MSL	1.157×10^{-5}
Bolshoy River	DEM - 0.1	2.314×10^{-3}
bog brook	DEM - 0.35	2.314×10^{-4}

High (14 April 2012) and low (01 September 2013) modelled heads are plotted along the W–E cross section (Figure 2) in Figure 10, which shows that modelled WTE is close to the DEM and the range of WTE is small. At the water divide in the centre of the bog, calculated WTE is below the DEM for part of the time; whereas at the western side of the bog it is substantially above the DEM. The flat sections of the WTE profiles on the western side of the cross section coincide with the large lake at that location.

Water fluxes through the bog complex

The modelled water fluxes through the acrotelm and catotelm layers vary substantially between spring and end of summer. For possible engineering applications (e.g. road construction through the bog) we examined the spring water fluxes through the N–S cross section shown in Figure 2. Average water discharge (per m; ± SD) in spring was 8.13×10^{-5} ($\pm 5.22 \times 10^{-5}$) $m^3\ s^{-1}$ through hollows, 2.26×10^{-6} ($\pm 1.75 \times 10^{-6}$) $m^3\ s^{-1}$ through ridges and ryam, 1.33×10^{-6} ($\pm 1.54 \times 10^{-6}$) $m^3\ s^{-1}$ through the entire catotelm and 2.3×10^{-6} ($\pm 7.41 \times 10^{-7}$) $m^3\ s^{-1}$ through the mineral sublayer (Figure 11). In other words, more than 90 % of the water flows through the acrotelm layer in hollows.

The ridges of ridge-hollow complexes act as barriers to water flow. A rainfall event or snowmelt peak causes the modelled water level upstream of a ridge to rise by 5−10 cm and thereby increases the vertically downward (Z) flux by 20−25 mm d^{-1}, while downstream of the ridge the (delayed) upward flux increases by 1−2 mm d^{-1} (Figure 12). The residence time of water moving along the west−east cross section, calculated using the calculated spring water fluxes, is shown in Figure 10. It takes about 200 years for water to reach the eastern margin of the bog if it starts from the vicinity of the water divide, but only 40 days if its journey begins halfway between the water divide and the margin. The much lower fluxes occurring later in the season were not considered in this analysis; the corresponding residence times should be longer.

Over the period 01 January 2009 to 31 October 2016, the calculated average discharge (± SD) of the bog brook at the eastern margin of the bog complex (Figure 2) was 4.58×10^{-3} ($\pm 6.83 \times 10^{-4}$) $m^3\ s^{-1}$, and that of the acrotelm was 1.64×10^{-3} ($\pm 1.5 \times 10^{-4}$) $m^3\ s^{-1}$. For this analysis, discharge from the bog brook was calculated as the sum of modelled discharge via all brook drains upstream of the steep bog margin (Figure 13).

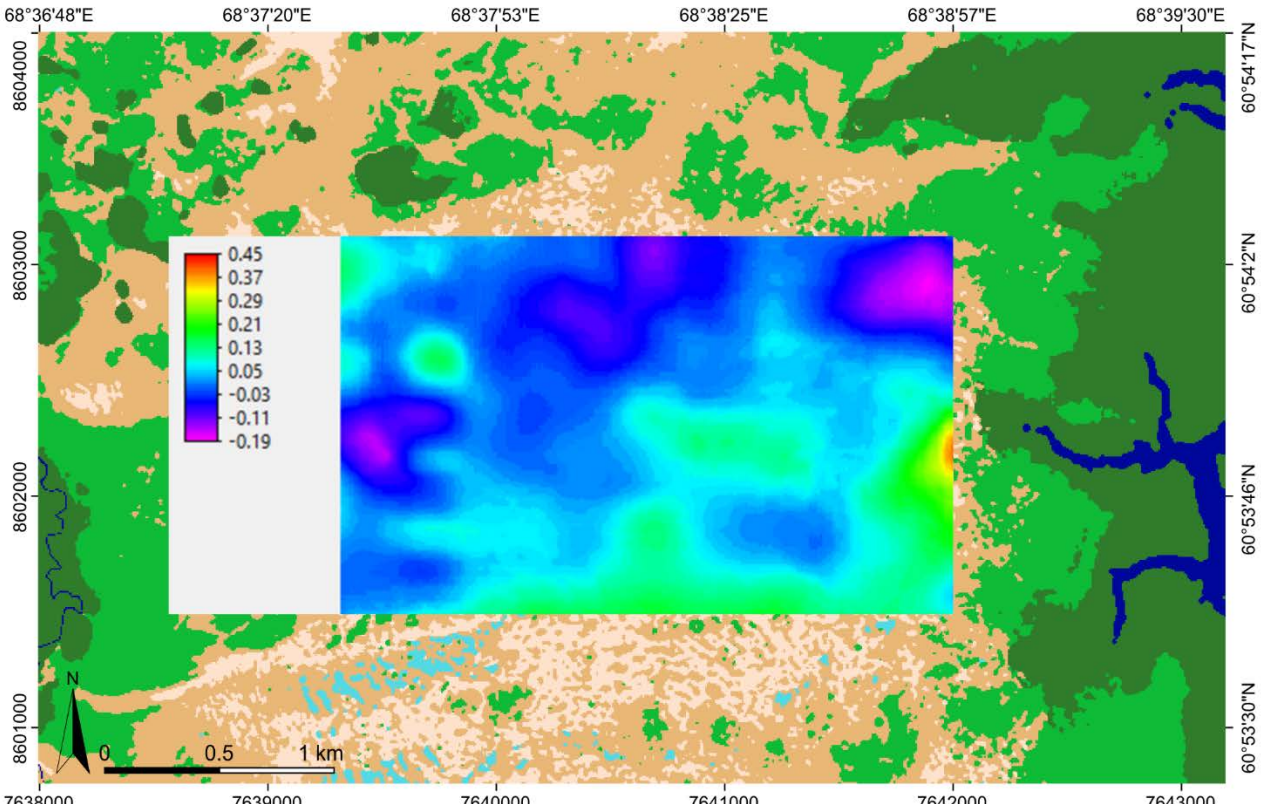

Figure 8. Steady state modelling result: water level in m above (> 0) or below (< 0) DEM in a selected central part of the model area. Mean difference = 0.025 m, SD = 0.073 m. Background: map of land unit types (Figure 2).

Dissolved organic carbon (DOC)

The DOC concentrations measured in the bog brook (Figure 2) are shown in Figures 14 and 15. DOC concentration decreases just after the beginning of snowmelt (in May), then increases steeply from the end of May (from mid-June in 2016) and finally stabilises later in the summer season. The highest concentrations were measured in the wet years 2011 and 2012, when WTE in the bog was highest. The clear dips in DOC concentration during spring seem to follow brook discharge (Q_b) but are shifted in time, resulting in weak correlation between Q_b and DOC concentration. However, when data collected in spring (before 10 July) were excluded, a significant linear regression ($R^2 = 0.58$, $N = 24$, $p = 0.035$) emerged.

Figure 14 presents the dynamics of DOC in the bog brook as calculated from the regression function. The mean DOC concentration of the brook water (± SD) was 42.82 ± 10.48 g m^{-3}. The effective catchment area (A) of the brook was calculated by dividing the average brook discharge (4.58×10^{-3} m^3 s^{-1}) by the sum of recharge (1.45×10^{-8} m m^{-2} s^{-1}) and percolation loss (-4.05×10^{-9} m m^{-2} s^{-1}). Based on the resulting A (438,277 m^2), the DOC export per day was 0.039 g m^{-2}, or for a growing season of 200 days the DOC loss from the area was 7.7 g m^{-2} y^{-1}.

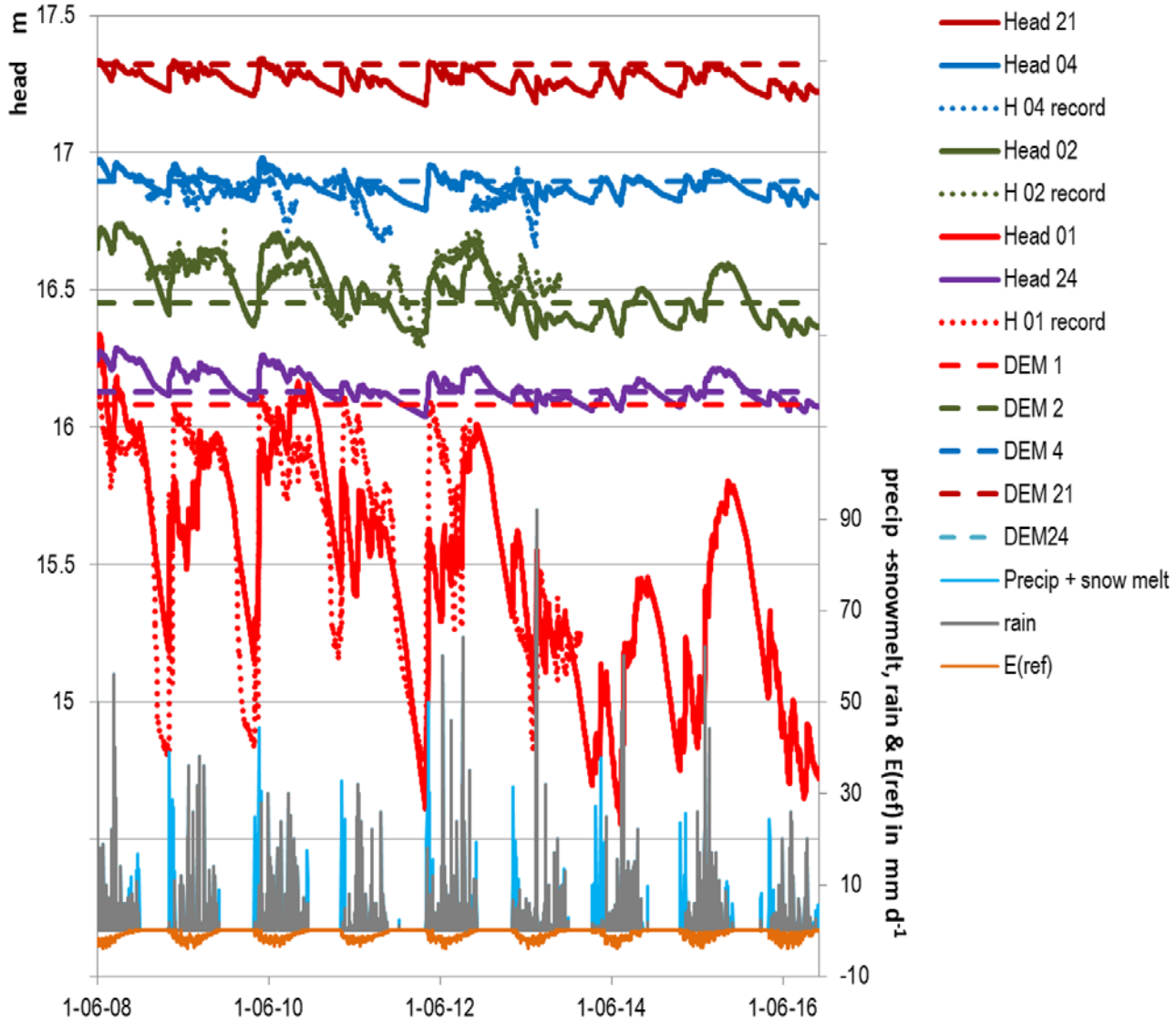

Figure 9. Dynamics of water level at five points within the model area (for locations see Figure 2). Head = modelled water level; DEM = top of Layer B. Y-axis: elevation in m above MSL; E(ref): reference evapotranspiration (Makkink) (= E_{ref} from Equations 1 and 2). Snowmelt, rain and E(ref) in mm d^{-1}.

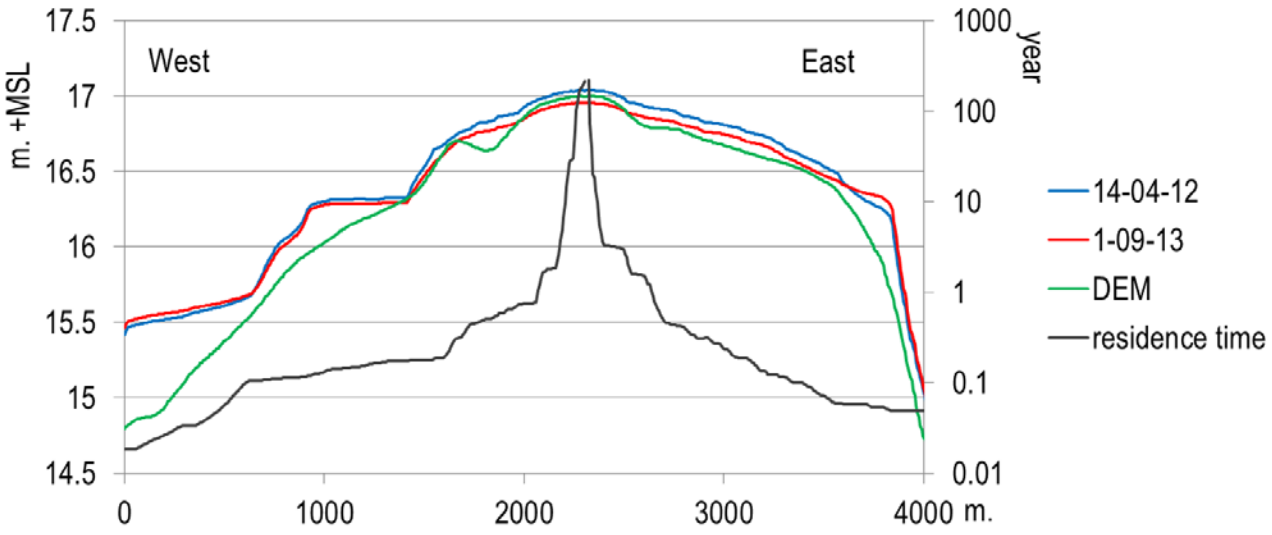

Figure 10. Modelled heads and residence time in the west–east cross section identified in Figure 2. Green line: surface; blue line: spring high water level (14 Apr 2012); red line: end of summer low water level (01 Sep 2013); grey line: residence time (right-hand Y-axis) based on spring water fluxes in Layers A and B.

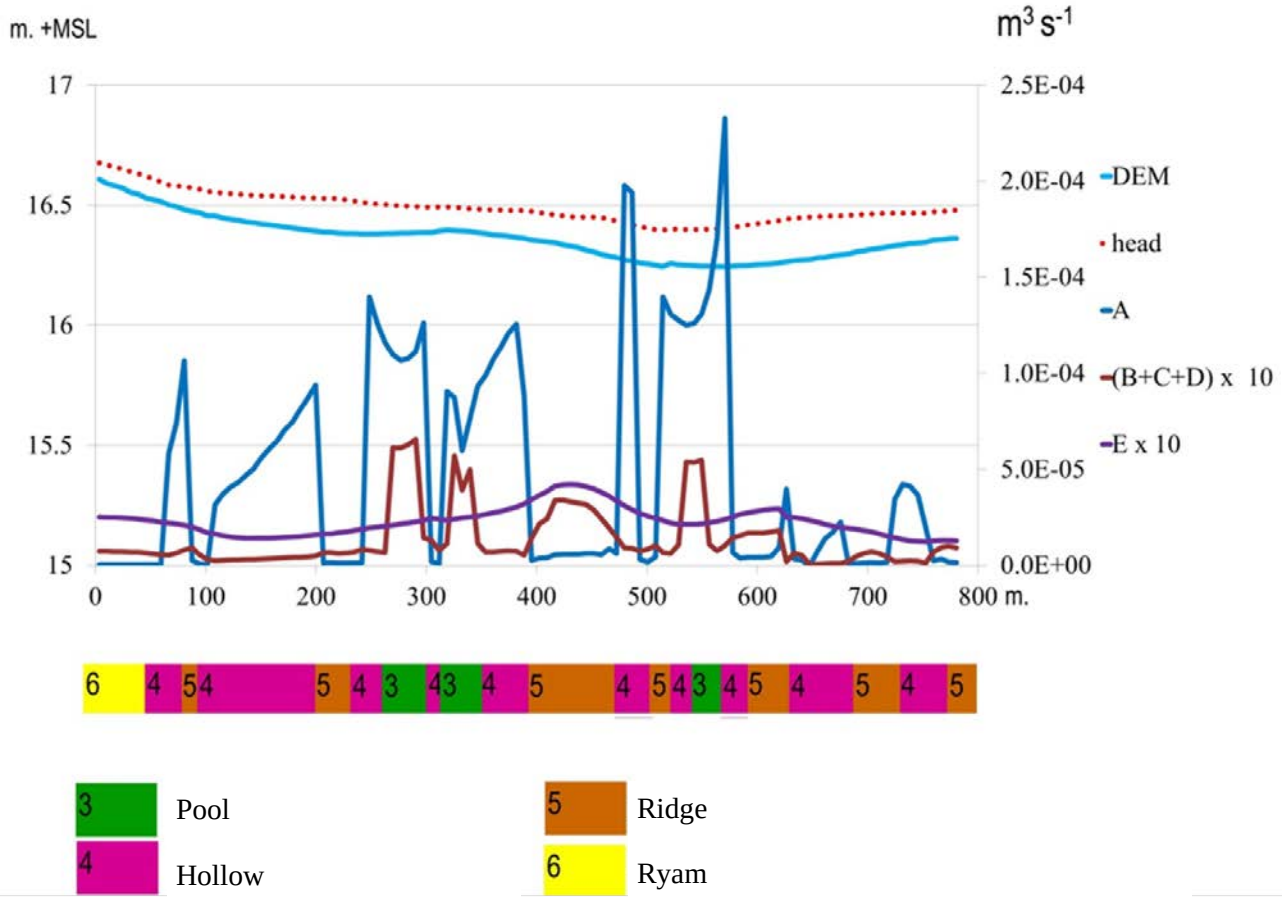

Figure 11. Water fluxes on 14 Apr 2012 across the north–south cross section identified in Figure 2, by model layer and land unit type (LUT). LUTs are indicated by the horizontal bar below the X (distance) axis. The left-hand Y-axis shows elevation (m above MSL) of the DEM (top of Layer B / catotelm) and WTE (head) (smooth upper plotted lines). The right-hand Y-axis shows eastward flux in $m^3 s^{-1}$ per m of cross section for Layers A, (B, C, D) and E (irregular lower plotted lines). Fluxes for (B+C+D) and E are multiplied by 10.

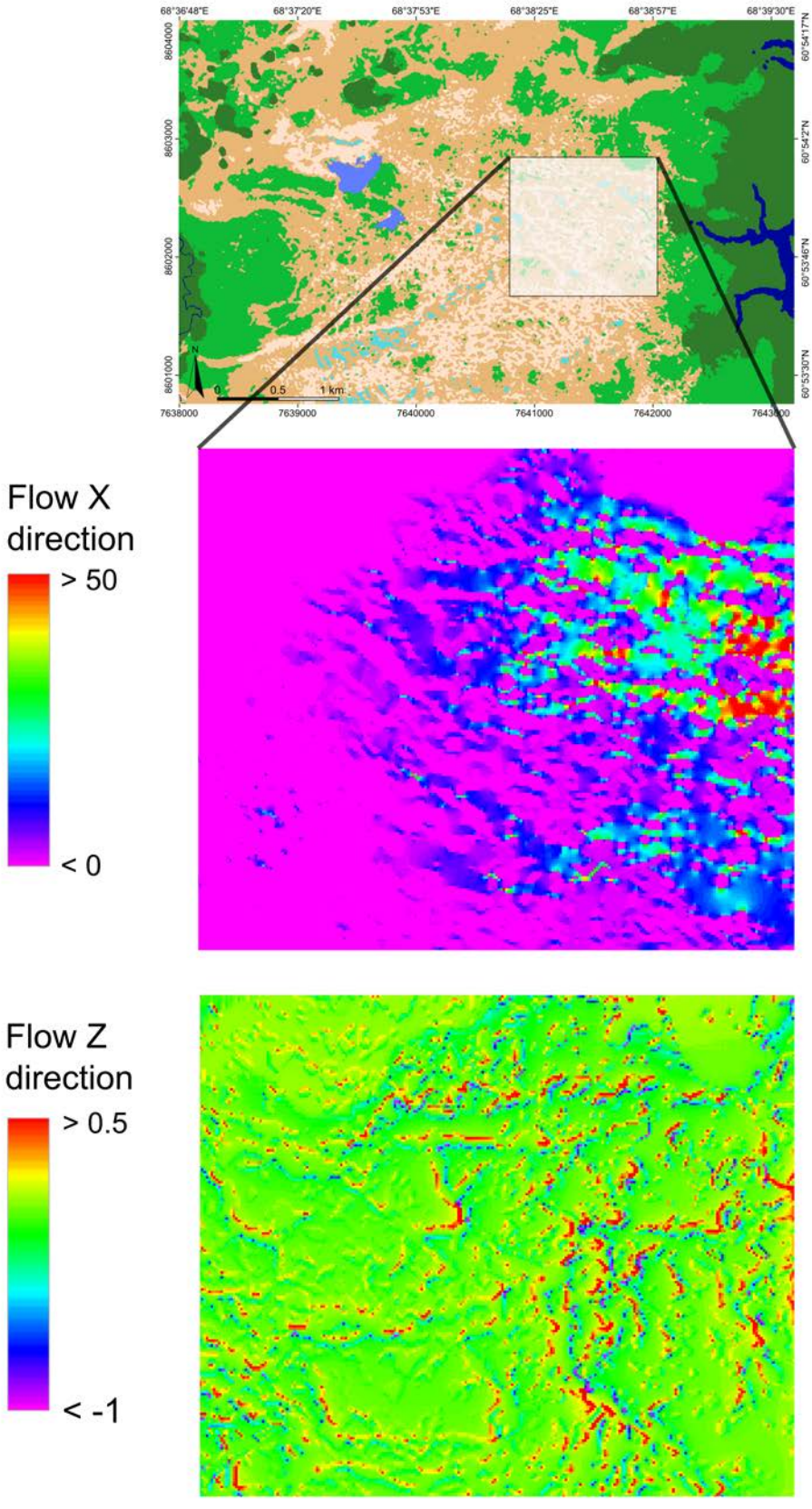

Figure 12. Selection of results maps showing modelled water fluxes for 29 June 2010. Flow X is eastward water flow (to the right) through Layer A (acrotelm), in $m^3\ d^{-1}$ per cell-side (50 = 7.1 $m^3\ d^{-1}$ per m); Flow Z is water flow from Layer A to Layer B (values > 0 indicate downward flow), in $m^3\ d^{-1}$ per cell-base (0.5 = 0.01 $m^3\ d^{-1}$).

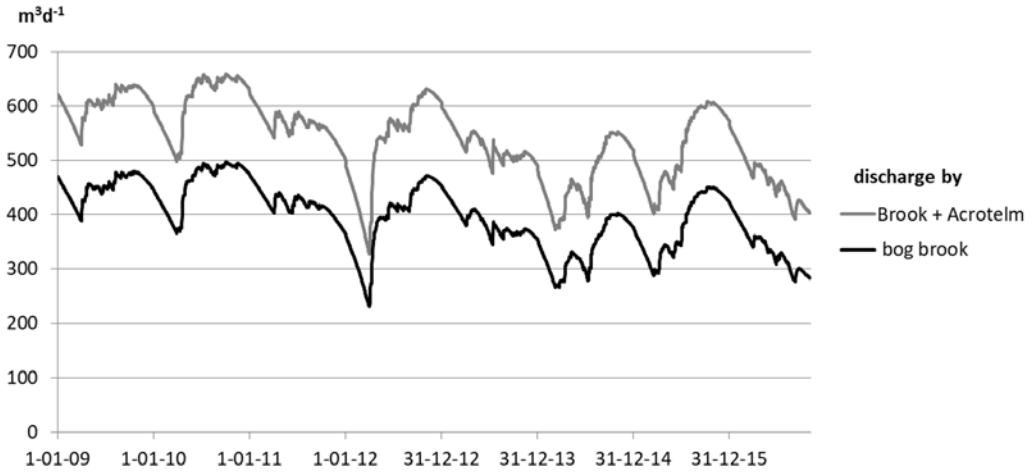

Figure 13. Dynamics of discharge from the bog brook, 2009–2016, measured directly (at location Q in Figure 2) and indirectly on the basis of modelled runoff through the acrotelm (Layer A).

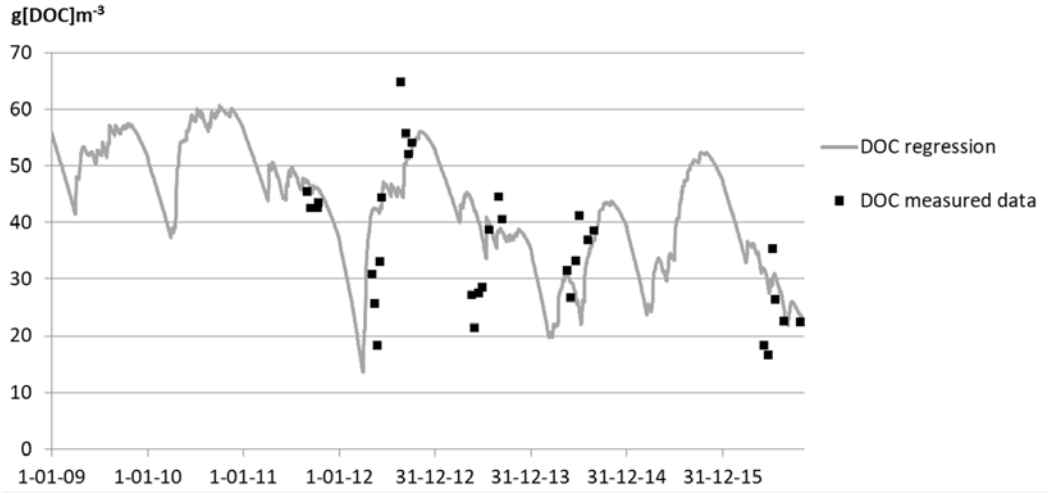

Figure 14. Measured DOC concentrations (black dots) at the outlet of the bog brook (Location Q in Figure 2) and dynamics of DOC concentration calculated using the regression function (grey line).

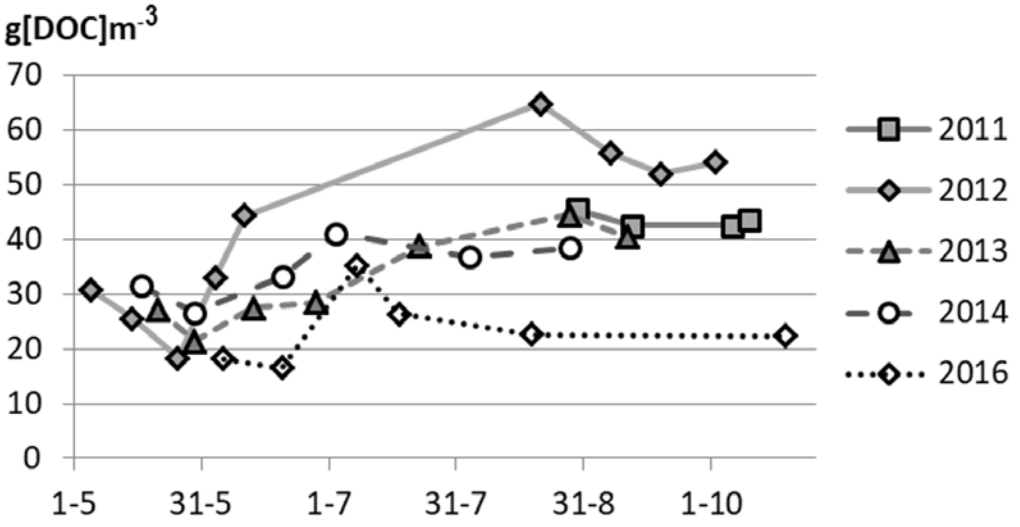

Figure 15. Dissolved Organic Carbon (DOC) concentrations measured at the outlet of the bog brook (location Q in Figure 2), 2011–2016.

DISCUSSION

Recharge

The lack of meteorological data other than those available from the meteorological station at Khanty-Mansiysk (MS-XM) forced us to simplify the calculation of evapotranspiration by using latitude-dependent radiation and the Makkink equation instead of the Penman-Monteith method. The Royal Dutch National Meteorological Institute (KNMI) uses the Makkink formula for E_{ref}, having proven its validity in comparison with other methods (de Bruin 1987, Alexandriss *et al.* 2008). However, it is impossible to assess whether our estimates of evapotranspiration deviated significantly from real values. Moreover, MS-XM is almost completely surrounded by the floodplains of the Rivers Ob (10–20 km wide) and Irtysh (10–15 km wide). The effects of this location on the precipitation, temperature and cloud cover data that we utilised have not been studied, but we can expect substantial implications for precipitation and temperature, particularly because the floodplains are inundated annually in late spring and early summer.

The predicted snowpack depth at Mukhrino during the period 2012–2016 was lower than measured at MS-XM, suggesting that our modelled spring snowmelt volumes for that period may be under-estimated. However, the range and fluctuations of recorded WTE at the bog margin were similar to those calculated by the transient model (compare 'Head 01' and 'H 01 record' in Figure 9), which supports the continued validity of the calculated snowmelt data. It is probable that the location of snow depth measurements or the conditions affecting snow deposition rates at MS-XM changed in 2012.

Hydraulic conductivity

The calibrated hydraulic conductivity values for Layer A (Table 3) are within the range of published values for the acrotelm (e.g. Ivanov 1957, 1981; Boelter 1968, Morris *et al*. 2015). Sensitivity analysis (see Appendix) showed that the use of high *K* values gave the best results. *K* values one order of magnitude lower resulted in a mean difference between calculated WTE and the top of Layer B (dH) of 0.3 m, which was regarded as unacceptable. The effect of changing the *K* value of Layer B was much less, indicating the importance of Layer A as the main water-conducting stratum.

The *K* values of model layers defined by iterations with the steady state model decrease from the top layer downward (Table 3). This trend is in accordance with published values (Boelter 1968, Rycroft *et al.* 1975, Ivanov 1981, Beckwith *et al.* 2003, Morris *et al.* 2015). Most published *K* values for peat are not suitable for use in modelling of large undisturbed bog complexes because they arise from measurements in more or less drained peatland or in blanket bog (not comparable to plateau mire), or because *K* data for the acrotelm is lacking. Detailed measurements of *K* in both the acrotelm and the catotelm have been done by Ivanov (1957, 1981) and recently by Morris *et al.* (2015). The *K* estimates we derived by calibration were at the high end of the range of published values (Figure 16), which is consistent with the finding of Bierkens & Weerts (1994) that groundwater models at block scale require higher values of horizontal hydraulic conductivity than are obtained from point measurements.

Water fluxes

The average water discharge (per m) through the N–S cross section in spring was 91 % through hollows, 2.0 % through ridges and ryam, 2.6 % through the entire catotelm and 4.6 % through the mineral sublayer. This reveals that water discharge in this cross section occurs mainly by flow through the acrotelm layer. This should be noted by engineers responsible for calculation of dimensions of bridges and culverts when aiming to avoid unwanted hydrological effects.

The pattern of LUTs affects the water flow substantially (Holden *et al.* 2008). The highest modelled flows occur through lakes and the hollows of ridge-hollow complexes. Ridges are barriers to water flow (Oosterwoud *et al*. 2017, van der Schaaf 1999, van der Ploeg 2012) The implementation of a top 'air layer' made it possible to model these effects. Water level rise caused by snowmelt or rainfall events led to increased infiltration upstream of ridges and smaller, but longer lasting, release of extra peat water downstream of ridges. This process supports the requirement for a model cell size which corresponds to the width of the ridges. The 'air layer' also enabled us to cope with the problem of bog surface movements (Roulet 1991, Kellner & Halldin 2002) in hollows and poor fen. The rise of floating vegetation with increasing WTE was mimicked by modelled WTE rising above the DEM.

The much lower fluxes occurring later in the season were not accounted for in calculating residence time, which may cause under-estimation of travel times. In particular, the water flow through Layer A (acrotelm) of ryam is comparatively small or even zero in dry periods.

The implementation of a temporarily frozen layer (top of catotelm) caused a general rise in WTE

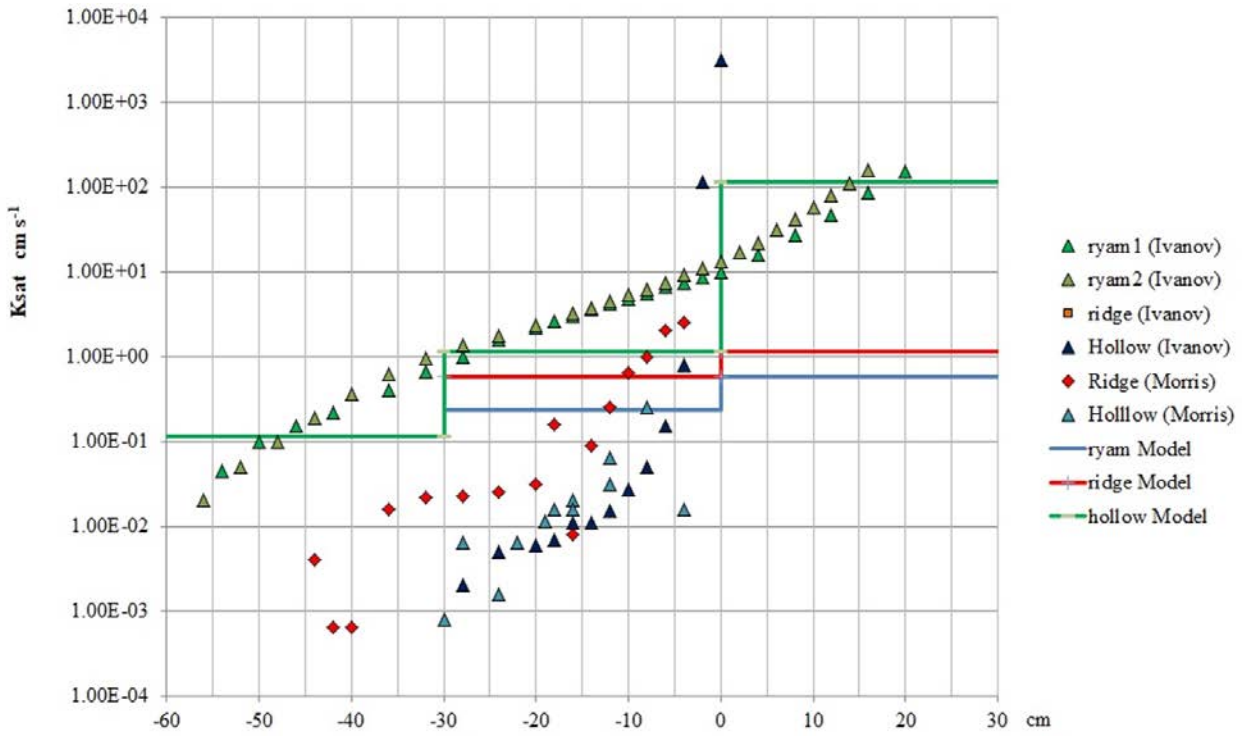

Figure 16. Hydraulic conductivity (K_{sat}) of acrotelm (depth > 0 cm on X-axis) and of catotelm (depth < 0 cm) measured by Ivanov (1957, 1981) and Morris *et al.* (2015). Ryam = raised bog. Solid lines: used in model.

of 0.005–0.02 m, enabling water flow through the acrotelm to occur more frequently. The water flows through the acrotelm over the entire bog area, although mostly through hollows and pools. The brook at the bog margin drains only a small part of the cross section shown in Figure 11. The modelled discharge of the bog brook ($4.58 \pm 6.83 \times 10^{-3}$ m^3 s^{-1}) was comparable to the average ($4.55 \pm 4.24 \times 10^{-3}$ m^3 s^{-1}) recorded outflow at the weir in 2008 (Bleuten & Fillippov 2008). In 2009 the weir was broken and the interception channel became leaky, making further observations unreliable.

Dissolved organic carbon (DOC)

The measured DOC concentrations varied substantially from year to year. Compared to 2014, the year 2012 was relatively wet with higher WTE and water flow velocities. Like Fraser *et al.* (2001) and Campeau *et al.* (2017) we observed a clear drop in DOC concentration in spring, which can be explained by the discharge of meltwater while the subsoil is frozen. Later, there was less dilution from snowmelt and DOC increased (Figure 14).

High WTE in summer caused increased flow rates, which resulted in relatively short residence time and increased DOC export. Longer residence time may enhance DOC concentration because the water is in contact with DOM and peat for longer, but also facilitates C-oxidation which tends to reduce DOC concentrations (Tang *et al.* 2018).

The calculated average DOC export of 7.7 g m^{-2} y^{-1} is within the range reported from Canada (8.1−7.0 g m^{-2} y^{-1}; Roulet *et al.* 2007) and unfrozen Swedish fen mires (14.9 g m^{-2} y^{-1}; Olefeldt & Roulet 2012). The latter authors observed much lower DOC export from palsa mires and bogs, which can be explained by the presence of permafrost in both of these mire types at their study location. Campeau *et al.* (2017) analysed streamwater from a northern Swedish mire complex similar to ours and came to an export rate of 12 g m^{-2} y^{-1}. To improve our understanding of the processes underlying DOC export, additional modelling of residence times as well as sampling schemes which are more detailed in space and time, will be required.

ACKNOWLEDGEMENTS

We thank Prof. Dr Marc Bierkens for his critical reading and improvements of the manuscript, Dr Frances Dunn for English proofreading, two anonymous reviewers and the editors. Part of the study was funded by Yugra State University under Project № 13-01-20/26.

AUTHOR CONTRIBUTIONS

Hydrological fieldwork was performed jointly by EZ and WB. EZ did the DOC sampling and analyses, peat drillings and interpretations. The preparation of model input data and hydrological modelling was done by WB with contributions from EZ (DEM) and OS (PCRaster-Modflow). WB wrote the manuscript with contributions from EZ and OS.

REFERENCES

Alekseychik, P., Mammarella, I., Karpov, D., Dengel, S., Terentieva, I., Sabrekov, A., Glagolev, M., Lapshina, E. (2017) Net ecosystem exchange and energy fluxes measured with the eddy covariance technique in a western Siberian bog. *Atmospheric Chemistry and Physics*, 17, 9333–9345, doi.org/10.5194/acp-17-9333-2017

Alexandriss, S., Stricevic, R., Petkovic, S. (2008) Comparative analysis of reference evapotranspiration from the surface of rain fed grass in central Serbia, calculated by six empirical methods against the Penman-Monteith formula. *European Water*, 21/22, 17–28.

Allen, R.G., Pereira, L.S., Raes, D., Smith, M. (1998) *Crop Evapotranspiration: Guidelines for Computing Crop Water Requirements*. Irrigation and Drainage Paper 56, Food and Agriculture Organization of the United Nations (FAO), Rome, 15 pp.

Baird, A.J., Morris, P.J., Belyea, L.R. (2012) The DigiBog peatland development model 1: rationale, conceptual model, and hydrological basis. *Ecohydrology*, 5, 242–255.

Baldocchi, D., Falge, E., Gu, L.H., Olson, R., Hollinger, D., Running, S., Anthoni, P., Bernhofer, C., Davis, K., Evans, R., Fuentes, J., Goldstein, A., Katul, G., Law, B., Lee, X.H., Malhi, Y., Meyers, T., Munger, W., Oechel, W., Paw, U.K.T., Pilegaard, K., Schmid, H.P., Valentini, R., Verma, S., Vesala, T., Wilson, K., Wofsy, S. (2001) FLUXNET: a new tool to study the temporal and spatial variability of ecosystem scale carbon dioxide, water vapor, and energy flux densities. *Bulletin of the American Meteorological Society*, 82, 2415–2434.

Beckwith, C.W., Baird, A.J., Heathwaite, L.A. (2003) Anisotropy and depth-related heterogeneity of hydraulic conductivity in a bog peat. II: modelling the effects on groundwater flow. *Hydrological Processes*, 17, 103–113.

Belyea, L.R., Clymo, R.S. (2001) Feedback control of the rate of peat formation. *Proceedings of the Royal Society of London: Biological Sciences*, 268, 1315–1321.

Belyea, L.R., Malmer, N. (2004) Carbon sequestration in peatland: patterns and mechanisms of response to climate change. *Global Change Biology*, 19, 1043–1052.

Bierkens, M.F.P., Weerts, J.T. (1994) Block hydraulic conductivity of cross-bedded fluvial sediments. *Water Resources Research*, 30(10), 2665–2678, doi.org/10.1029/94WR01049.

Bleuten, W., Bierkens, M.F.P. (2015) Lysimeteronderzoek naar de evapotranspiratie van riet en els in een trilveen bij Schalkwijk U. (Lysimeter study of evapotranspiration by reed and alder in a quagmire near Schalkwijk U.). *Stromingen*, 23(3), 6–24 (in Dutch).

Bleuten, W., Filippov, I. (2008) Hydrology of mire ecosystems in central West Siberia: The Mukhrino field station. In: Glagolev, M.V., Lapshina, E.D. (eds.) *Dynamics of Environment and Global Climate Change*, Volume 1, Transactions of UNESCO Department of Yugorsky State University, NSU, Novosibirsk, 208–224. ISBN 978-5-94356-749-0.

Boelter, D.H. (1968) Important physical properties of peat materials. *Proceedings of the Third International Peat Congress*, International Peat Society, Quebec, Canada, 150–154.

Borren, W., Bleuten, W. (2006) Simulating Holocene carbon accumulation in a western Siberian watershed mire using a three-dimensional dynamic modelling approach. *Water Resources Research*, 42, W12413, doi:10.1029/2006 WR004885.

Broder, T., Biester, H. (2015) Hydrologic controls on DOC, As and Pb export from a polluted peatland - the importance of heavy rain events, antecedent moisture conditions and hydrological connectivity. *Biogeosciences*, 12, 4651–4664.

Campeau, A., Bishop, K.H., Billett, M.F., Garnett, M.H., Loudon, H., Leach, J.A., Nilsson, M.B., Öquist, M.G., Wallin, B. (2017) Aquatic export of young dissolved and gaseous carbon from a pristine boreal fen: Implications for peat carbon stock stability. *Global Change Biology*, 2017 (23), 5523–5536, doi.org/10.1111/gcb.13815.

Chaudhary, N., Miller, P.A., Smith, B. (2017) Modelling Holocene peatland dynamics with an individual-based dynamic vegetation model. *Biogeosciences*, 14, 2571–2596.

Christensen, T.R., Jonasson, S., Callaghan, T.V., Havström, M. (1995) Spatial variation in high-latitude CH_4 flux along a transect across Siberian and Eurasian tundra environments. *Journal of Geophysical Research*, 100, 21035–21045.

Cresto Aleina, F., Runkle, B.R.K., Kleinen, T., Kutzbach, L., Schneider, J., Brovkin, V. (2015) Modeling micro-topographic controls on boreal peatland hydrology and methane fluxes. *Biogeosciences*, 12, 5689–5704.

de Bruin, H.A.R. (1987) From Penman to Makkink. In: Hooghart, J.C. (ed.) *Evaporation and Weather*, Proceedings and Information 39, TNO Committee on Hydrological Research, Netherlands Organization for Applied Scientific Research, The Hague, 5–31. ISBN 90-6743-117-6.

Dimitrov, D.D., Grant, R.F., Lafleur, P.M., Humphreys, E.R. (2010) Modeling the subsurface hydrology of Mer Bleue Bog. *Soil Science Society of America Journal*, 74(2), 680–694.

Dinsmore, K., Billett, M., Dyson, K. (2013) Temperature and precipitation drive temporal variability in aquatic carbon and GHG concentrations and fluxes in a peatland catchment. *Global Change Biology*, 19(7), 2133–2148.

Doherty, J. (2001) Improved calculations for dewatered cells in MODFLOW. *Groundwater*, 39, 863–869.

Dyukarev, E.A., Godovnikov, E.A., Karpov, D.V., Kurakov, S.A., Lapshina, E.D., Filipov, I.V., Filippova, N.V., Zarov, E.A. (2019) Net ecosystem exchange. Gross primary production and ecosystem respiration in ridge-hollow complex at Mukhrino bog. *Geography, Environment, Sustainability*, 12(2), 227–244, doi:10.24057/2071-9388-2018-77.

Edom, F., Munch, A., Dittrich, I., Keßler, K., Peters, R. (2010) Hydromorphological analysis and water balance modelling of ombro- and mesotrophic peatlands. *Advances in Geosciences*, 27, 131–137.

Eppinga, M.B., Rietkerk, M., Borren, W., Lapshina, E.D., Bleuten, W., Wassen, M.J. (2008) Regular surface patterning of peatlands: confronting theory with field data. *Ecosystems*, 11, 520–536, doi:10.1007/s10021-008-9138-z.

Feddes, R.A. (1987) Crop factors in relation to Makkink reference-crop evapotranspiration. In: Hooghart, J.C. (ed.) *Evaporation and Weather*, Proceedings and Information 39, TNO Committee on Hydrological Research, Netherlands Organization for Applied Scientific Research, The Hague, 33–45. ISBN 90-6743-117-6.

Fraser, C.J.D., Roulet, N.T., Lafleur, M. (2001) Groundwater flow patterns in a large peatland. *Journal of Hydrology*, 246, 142–154.

Frolking, S., Roulet, N.T., Tuittila, E.S., Bubier, J.L., Quillet, A., Talbot, J., Richard, P.J.H. (2010) A new model of Holocene peatland net primary production, decomposition, water balance, and peat accumulation. *Earth System Dynamics*, 1, 1–21, doi:10.5194/esd-1-1.

GOST (1991) *Soils. Methods for Determination of Organic Matter*. State Standard 26213-91, State Committee on Standards of the former USSR, Moscow, 8 pp. (in Russian).

Gvozdetskii, N.A., Krivolutskii, A.E., Makunina, A.A. (1973) *Fiziko-geograficheskoe rajonirovanie Tyumenskoj oblasti* (*Physical and Geographical Zoning of the Tyumen Region*). Moscow State University Publishing House, 9–28 (in Russian).

Harbaugh, A.W., Banta, E.R., Hill, M.C., McDonald, M.G. (2000) *MODFLOW-2000, The U.S. Geological Survey Modular Ground-Water Model - User Guide to Modularization Concepts and the Ground-Water Flow Process*. Open-File Report (20)00-92, U.S. Geological Survey, Reston, VA, viii+121 pp. doi:10.3133/ofr200092.

Hemond, H.F., Goldman, J.C. (1985) On non-Darcian water flow in peat. *Journal of Ecology*, 73, 579–584.

Hilbert, D.W., Roulet, N., Moore, T. (2003) Modelling and analysis of peatlands as dynamical systems. *Journal of Ecology*, 88(2), 230–242.

Holden, J., Burt, T.P. (2003) Hydrological studies on blanket peat: The significance of the acrotelm-catotelm model. *Journal of Ecology*, 91(1), 86–102.

Holden, J., Kirkby, M.J., Lane, S.N., Milledge, D.G., Brookes, C.J., Holden, V., McDonald, T. (2008) Overland flow velocity and roughness properties in peatlands. *Water Resources Research*, 44, W06415, doi:10.1029/2007WR006052.

Howie, A., Hebda, R.J. (2018) Bog surface oscillation (mire breathing): A useful measure in raised bog restoration. *Hydrological Processes*, 32(11), 1518–1530, doi:10.1002/hyp.11622.

Huang, Y., Jiang, J., Ma, S., Ricciuto, D., Hanson, P.J., Luo, Y. (2017), Soil thermal dynamics, snow cover, and frozen depth under five temperature treatments in an ombrotrophic bog: Constrained forecast with data assimilation. *Biogeosciences*, 122, 2046–2063, doi:10.1002/ 2016JG003725.

Ingram, H.A.P. (1978) Soil layers in mires: functioning and terminology. *Journal of Soil Science*, 29, 224–227.

Ivanov K.E. (1957) *Osnovy gidrologii bolot lesnoj zony* (*Fundamentals of Peatland Hydrology in the Forest Zone*). Gydrometeoizdat, Leningrad, 499 pp. (in Russian).

Ivanov, K.E. (1981) *Water Movement in Mirelands*. Academic Press, London, xxviii+278 pp.

Kellner, E., Halldin, S. (2002) Water budget and surface-layer water storage in a *Sphagnum* bog in central Sweden. *Hydrological Processes*, 16, 87–

103, doi:10.100/hyp.286.

Kormann, R., Meixner, F.X. (2001) An analytical footprint model for neutral stratification. *Boundary-Layer Meteorology*, 99, 207–224.

Kosykh, N.P., Mironycheva-Tokareva, N.P., Peregona, A.M., Parshina, E.K. (2008) Biological productivity of bogs in the middle taiga subzone of Western Siberia. *Russian Journal of Ecology*, 39(7), 466–474.

Kutzbach, L., Wagner, D., Pfeiffer, E.M. (2004) Effect of micro relief and vegetation on methane emission from wet polygonal tundra, Lena Delta, Northern Siberia. *Biogeochemistry*, 69, 341–362.

Laitinen, J., Rehell, S., Huttunen, A., Tahvanainen, T., Heikkilä, R., Lindholm, T. (2007) Mire systems in Finland — special view to aapa mires and their water-flow pattern. *Suo*, 58(1), 1–26, ISSN 0039-5471.

Lapen, D.R., Price, J.S., Gilbert, R. (2005) Modelling two-dimensional steady-state groundwater flow and flow sensitivity to boundary conditions in blanket peat complexes. *Hydrological Processes*, 19, 371–386, doi: 10.1002/hyp.1507.

Leach, J.A., Larsson, A., Wallin, M.B., Nilsson, M. B., Laudon, H. (2016) Twelve year interannual and seasonal variability of stream carbon export from a boreal peatland catchment. *Biogeosciences*, 121, 1851–1866.

Mackin, F., Flynn, R., Barr, A., Fernadez-Valverde, F. (2017) Use of geographical information system-based hydrological modelling for development of a raised bog conservation and restoration programme. *Ecological Engineering*, 106, 242–252.

Makkink, G.F. (1957) Testing the Penman formula by means of lysimeters. *Journal of the Institute of Water Engineering*, 11, 277–288.

McCarter, C.P.R., Price, J.S. (2017) Experimental hydrological forcing to illustrate water flow processes of a subarctic ladder fen peatland. *Hydrological Processes*, 318, 1578–1589.

Mezbahuddin, M., Grant, R.F., Flanagan, L.B. (2016) Modeling hydrological controls on variations in peat water content, water table depth, and surface energy exchange of a boreal western Canadian fen peatland. *Biogeosciences*, 121(8), 2216–2242.

Moore, T.R., Roulet, N.T., Waddington, J.M. (1998) Uncertainty in predicting the effect of climatic change on the carbon cycling of Canadian peatlands. *Climatic Change*, 40(2), 229–245, doi.org/10.1023/A:1005408719297.

Moors, E.J. (2008) Evaporation. In: Bierkens, M.F.P., Dolman, A.J., Troch, P.A. (eds.) *Climate and the Hydrological Cycle*, IAHS Special Publications 8, IAHS Press, Wallingford, 344 pp.

Morris, P.J., Baird, A.J., Belyea, L.R. (2015) Bridging the gap between models and measurements of peat hydraulic conductivity. *Water Resources Research*, 51, 5353–5364, doi:10.1002/ 2015WR017264.

Olefeldt, D., Roulet, N.T. (2012) Effects of permafrost and hydrology on the composition and transport of dissolved organic carbon in a subarctic peatland complex. *Journal of Geophysical Research*, 117, G01005, doi: 10.1029/2011JG001819.

Olefeldt, D., Roulet, N., Giesler, R., Persson, A. (2013) Total waterborne carbon export and DOC composition from ten nested subarctic peatland catchments—Importance of peatland cover, groundwater influence, and inter-annual variability of precipitation patterns. *Hydrological Processes*, 27(16), 2280–2294.

Oosterwoud, M., van der Ploeg, M., van der Schaaf, S., van der Zee, S. (2017) Variation in hydrologic connectivity as a result of microtopography explained by discharge to catchment size relationship. *Hydrological Processes*, 31, 2683–2699, doi.org/10.1002/hyp. 11164.

Price, J.S. (2003) Role and character of seasonal peat soil deformation on the hydrology of undisturbed and cutover peatlands, *Water Resources Research*, 39(9), 1241, doi:10.1029/2002WR 001302.

Reeve, A.S., Warzocha, J., Glaser, P.H., Siegel, D.I. (2001) Regional ground-water flow modelling of the Glacial Lake Agassiz Peatlands, Minnesota. *Journal of Hydrology*, 243, 91–100.

Roulet, N.T. (1991) Surface level and water table fluctuations in a subarctic fen. *Arctic and Alpine Research*, 23(3), 303–310, doi.org/10.1080/ 00040851.1991.12002849.

Roulet, N.T., Lafleur, P.M., Richard, P.J.H., Moore, T.R., Humphreys, E.R., Bubier, J.I.L.L. (2007) Contemporary carbon balance and late Holocene carbon accumulation in a northern peatland. *Global Change Biology*, 13, 397–411, doi: 10.1111/j.1365-2486.2006.01292.x.

RP5.RU (2017) Weather archive in Khanty-Mansiysk (airport). Website, Raspisaniye Pogodi Ltd., St Petersburg. Online at: http://rp5.ru/ archive.php?wmo_id=23933&lang=ru, accessed 2017.

Rycroft, D.W., Williams, D.J.A., Ingram, H.A.P. (1975) The transmission of water through peat I: Review. *Journal of Ecology*, 63(2), 535–556.

Schmitz, O., Karssenberg, D., van Deursen, W.P.A., Wesseling, C.G. (2009) Linking external components to a spatio-temporal modelling framework: Coupling MODFLOW and PCRaster.

Environmental Modelling & Software, 249, 1088–1099, doi:10.1016/j.envsoft.2009.02.018.

Shi, X., Thornton, P.E., Ricciuto, D.M., Hanson P.J., Mao, J., Sebestyen, S.D., Griffiths, N.A., Bisht, G. (2015) Representing northern peatland micro-topography and hydrology within the Community Land Model. *Biogeosciences*, 12, 6463–6477.

Silvola, J., Alm, J., Ahlholm, U., Nykänen, H., Martikainen, P.J. (1996) CO_2 fluxes from peat in boreal mires under varying temperature and moisture conditions. *Journal of Ecology*, 84, 219–228.

Strack, M., Waddington, R.A., Bourbonniere, E., Kenny, L., Shaw, K., Whittington, P., Price, J.S. (2008) Effect of water table drawdown on peatland dissolved organic carbon export and dynamics. *Hydrological Processes*, 22, 3373–3385, doi:10.1002/hyp.6931.

Tang, J., Yurova, A.Y., Schurgers, G., Miller, P.A., Olin, S., Smith, B., Siewert, M.B., Olefeldt, D., Pilesjö, P., Poska, A. (2018) Drivers of dissolved organic carbon export in a subarctic catchment: Importance of microbial decomposition, sorption-desorption, peatland and lateral flow. *Science of the Total Environment*, 622–623, 260–274.

Turunen, J., Tahvanainen, T., Tolonen, K., Pitkanen, A. (2001) Carbon accumulation in West Siberian mires, Russia. *Global Biogeochemical Cycles*, 15, 285–296, doi:10.1029/2000 GB001312.

van der Ploeg, M.J. (2012) Microtopography as a driving mechanism for ecohydrological processes in shallow groundwater systems. *Vadose Zone Journal*, 11(3), doi:10.2136/vzj2011.0098.

van der Schaaf, S. (1999) *Analyses of the Hydrology of Raised Bogs in the Irish Midlands*. PhD thesis, University of Wageningen, The Netherlands, 375 pp. ISBN 90-5808-062-5.

Waddington, J.M., Quinton, W.L., Price. J.S., Lafleur, P.M. (2009) Advances in Canadian peatland hydrology, 2003–2007. *Canadian Water Resources Journal*, 34(20), 139–148.

Weiss, R., Shurpali, M.J., Sallantaus, T., Laiho, R., Laine, J., Alm, J. (2006) Simulation of water table level and peat temperatures in boreal peatlands. *Ecological Modelling*, 192, 441–456.

Whitfield, P.H., St-Hilaire, A., van der Kamp, G. (2009) Improving hydrological predictions in peatlands. *Canadian Water Resources Journal*, 344, 467–478.

Wu, Y., Verseghy, D.L., Melton, J.R. (2016) Integrating peatlands into the coupled Canadian Land Surface Scheme (CLASS) v3.6 and the Canadian Terrestrial Ecosystem Model (CTEM) v2.0. *Geoscientific Model Development*, 9, 2639–2663, https://doi.org/10.5194/gmd-9-2639-2016.

Yurova, A., Wolf, A., Sagerfors, J., Nilsson, M. (2007) Variations in net ecosystem exchange of carbon dioxide in a boreal mire: Modeling mechanisms linked to water table position. *Biogeosciences*, 112, G02025, doi:10.1029/2006 JG000342

Zarov, E.A. (2013) Vidy torfa verhovyh bolot i ih fiziko-khimicheskie svoistva (na primere bolotnogo massiva Mukhrno, KhMAO-Yugra) (Types of bog peat and their physicochemical properties (on the example of the Mukhrino peatland, KhMAO-Yugra)). In: *Problems of Rational Nature Management and the History of Geological Prospecting in Western Siberia*, Proceedings of the 1st regional youth conference named after V.I. Shpilman (25–26 Mar 2013, Museum of Geology, Oil and Gas, Khanty-Mansyisk), Editorial and Publishing Department of the Institute of Education Development, Khanty-Mansyisk, 118–121 (in Russian).

Submitted 14 Mar 2019, final revision 06 Dec 2019
Editors: Jonathan Price and Olivia Bragg

Author for correspondence:
Prof. Dr Wladimir Bleuten, Department of Physical Geography, Utrecht University, Vening Meinesz Building A, Princetonlaan 8a, 3584 CB Utrecht, The Netherlands. Tel: (+31) 30 2532749; E-mail: w.bleuten@uu.nl

Appendix: further information about Methods

Method for measurement of DOC

The DOC concentrations of water samples were measured with Tuirin's method for determination of soil organic carbon, modified to use a spectrophotometer (GOST 1991). Tuirin's method is based on the wet oxidation of organic matter by chromic acid and may be applied to water samples.

A potassium dichromate solution (13 M) was prepared by mixing 40 mg of $K_2Cr_2O_7.H_2SO_4$ with 1 dm^3 (1 L) of distilled water in a volumetric flask. The solution was then transferred to a ceramic beaker and diluted with 1 dm^3 of concentrated sulphuric acid (1M) over a period of 60–80 minutes to avoid overheating.

A calibration solution of Mohr's salt (0.1 M $(NH_4)_2Fe(SO_4)_2.6H_2O$) was prepared by mixing 40 mg of the salt with 700 cm^3 of sulphuric acid (1 M) and making up to 1 litre with distilled water. To check the salt concentration in the solution, 10 cm^3 of the Mohr's salt solution, 1 cm^3 of concentrated (1 M) sulphuric acid and 50 cm^3 of distilled water were mixed together in a 75–100 cm^3 Erlenmeyer flask and the mixture was titrated with 0.1 M potassium permanganate solution until a permanent light pink colour was obtained (three replications). The correction factor was calculated using the equation: $K = V_1/V$, where V_1 is the average volume (cm^3) of potassium permanganate solution used and V is the volume of Mohr's salt solution (10 cm^3 in this case).

For calibration, six solutions were prepared by mixing different volumes of the Mohr's salt solution (reducing agent) and distilled water (Table A1, test numbers 1–6) with 10 cm^3 of the potassium dichromate solution in 75–100 cm^3 Erlenmeyer flasks. All solutions were boiled in a water bath for one hour. The optical density of each mixture was then determined using a UV/Vis spectrophotometer (Lambda 35; Perkin Elmer, Waltham MA) at wavelength 590 nm and 1 cm of cell width, with comparison to zero-concentration solution. The relationship between optical density and the concentration of organic carbon is linear and provided in the standard.

Each (40 cm^3) filtered water sample from the bog brook was mixed with 10 cm^3 of the potassium dichromate solution and boiled in a water bath for one hour. Then, optical density was determined as above, the corresponding carbon concentration (m = mass in 40 cm^3 of sample) was derived using the calibration relationship, and the (corrected) organic carbon concentration (C; mg L^{-1}) was calculated using the equation: $C = m \cdot K \cdot 25$, where K is the correction factor. The relative error of this method is 20 % for 3 % of organic mass, 15 % for 3–5 % of organic mass 10 % for 5–15 % of organic mass.

Table A1. Solutions used for calibration.

Solutions	Test number					
	1	2	3	4	5	6
Water (cm^3)	40	39	38	36	32	30
Mohr's salt (cm^3)	0	1	2	4	8	10
Concentration of organic carbon (g m^{-3})	0	0.515	1.03	2.07	4.14	5.17

High resolution 3D groundwater modelling with PCRaster-MODFLOW

The groundwater model of the Mukhrino bog was developed using the Python programming language and the PCRaster-Modflow module (Schmitz *et al*. 2009). The input datasets that are required to set up the five-layer model are either spatial datasets (i.e. 2D raster maps) for each layer (e.g. elevation, drains, conductivities), or time series input files (e.g. recharge, temperature) for transient simulations.

PCRaster-MODFLOW provides a set of functions to specify the inputs required for MODFLOW packages (e.g. DIS, DRN, PCG) and to obtain output values as spatial datasets after a MODFLOW stress period has been executed. Raster maps of heads, X, Y and Z fluxes, drains, rivers and wells can be produced for each layer and for each time step. These results maps can be inspected simultaneously using the Aguila visualisation tool included in PCRaster.

The Mukhrino bog model uses the MODFLOW packages DIS, BAS, BCF, DRN, PCG and RCH. To avoid a large number of cells in the study area falling dry we needed to use the rewetting option provided within the BCF package (Doherty 2001). The flexibility of the Python script enables the modeller to change even fixed variables between time steps. This facility was employed to simulate a temporarily frozen model layer. For Layer B (catotelm), we changed the conductivity values when the daily temperature dropped below a threshold value and reset them when higher temperatures recurred.

The writing of output raster maps is runtime consuming but can be limited to particular layers or single variables, e.g. head and X fluxes only. When writing the full output of our transient model (spanning eight years) the runtime was 36 hours (2.3 GHz) and used 80 Gb of storage space.

Calculation of snowmelt water per day

For calculation of the volume of recharge by snowmelt per day we used a degree-day model, simplified after Huang *et al*. (2017) and Chaudhary *et al*. (2017) (Equation A3.1), to compute snowpack depth, sublimation and snowmelt. The model was calibrated with daily snow depth and temperature data provided by Meteorological Station Khanty-Mansyisk (MS-XM 1-01-2008 to 1-05-2008 (Figure A1). The snowpack depth was modelled well, but more important for hydrological modelling was the successful modelling of the snowmelt period and the snowmelt water volume per day.

Using the parameters derived for the calibration period, the whole period 2008–2016 was elaborated by forward modelling (Figure C2). For T < 0 °C:

$$Sd_t = Sd_{t-1} - (a + b)T_t + cP_t \qquad [A1]$$

where Sd is snow depth (cm), ($a\ T_t$) is snowmelt (cm) for T < 0 °C, $a = 0$, (bT_t) is ablation (cm) for T < 0 °C, $b = 0$, (cP_t) is snow deposition (cm), T is 24 h average temperature (°C), t is time step (day) and P is measured precipitation for T < 0 °C at MS-XM (cm d^{-1}). Parameter values were established as: $a = 1.6$, $b = 0.003$, $c = 0.25$.

The results of the snowpack model (Figure A2) beyond the period used for model calibration (2008) showed very good results for the period 2009–2012 (Y = 0.929X, $R^2 = 0.9266$). The results for the period 2012–2016 were less good (Y = 0.418X, $R^2 = 0.796$) although the trends of computed and measured snow depths were comparable in all winters. The mean results obtained by the snow model averaged over eight years were (mm y^{-1}): sublimation = 70 (SD: 10); snowmelt = 226 (SD: 90); snow = 607 (SD: 210); rainfall = 504 (SD: 98). We decided to use the data produced by the snow model.

Figure A1. Calibration of the degree-day model (2008). Snow depth in cm.

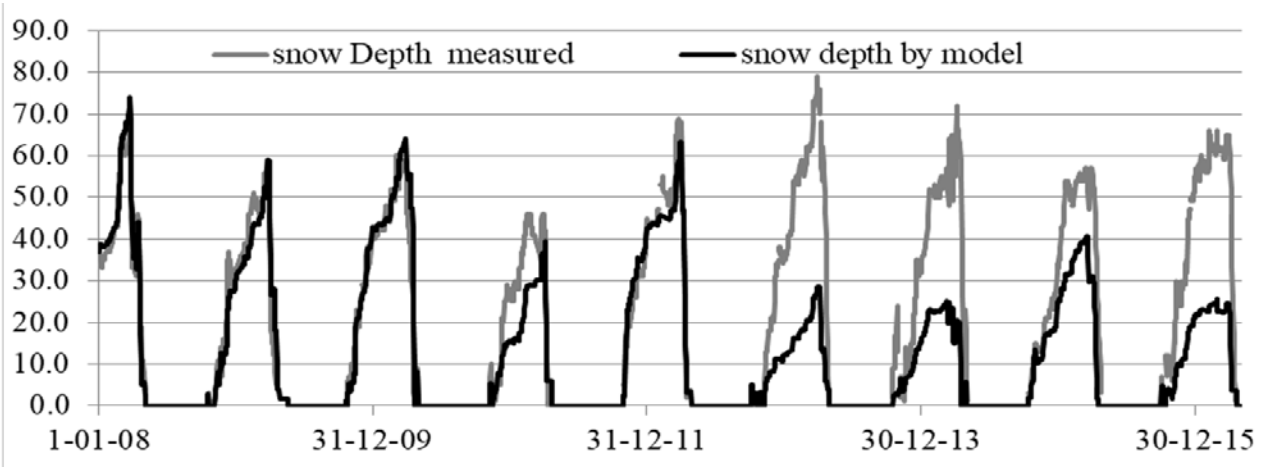

Figure A2. Modelled and measured snow depth, 2008–2016. Snow depth in cm.

Sensitivity analyses

Hydraulic conductivity (*K*) of the top layers of the model is the most important factor for water flow. The *K* values used were defined iteratively in the steady state model (SS-Mukhrino) by varying *K* and drain conductance Dc. The water level in the bog part of the model area should be close to the top of the catotelm (Layer B = DEM), as observed in the field. This was achieved by using very high *K* values. Figure A3 shows the effects of reducing *K* in Layers A and B within the bog on the averaged water levels (head) within the selected central model area. The average water level rose by 0.13 m when *K* values were reduced to one-fifth of the initial values, and even by 0.27 m with *K* values one order of magnitude lower than initial. The effect of changing the *K* values of both Layers A and B resulted in only a slightly greater effect, the water level rising by 0.18 m and 0.36 m, respectively (Figure A3).

The effect of changing recharge is much smaller. Increasing recharge by 10 % and 20 % resulted in changes in water level of 5 cm and 7 cm, respectively. Reducing recharge seemed to improve the model results, but MODFLOW could not converge and produced unacceptably increased water balance discrepancies (Figure A4). These discrepancies can be compensated during model iterations by adapting the drain conductance, which is the counterpart of recharge. However, in the case of raised water levels due to higher recharge, *K* should also be increased.

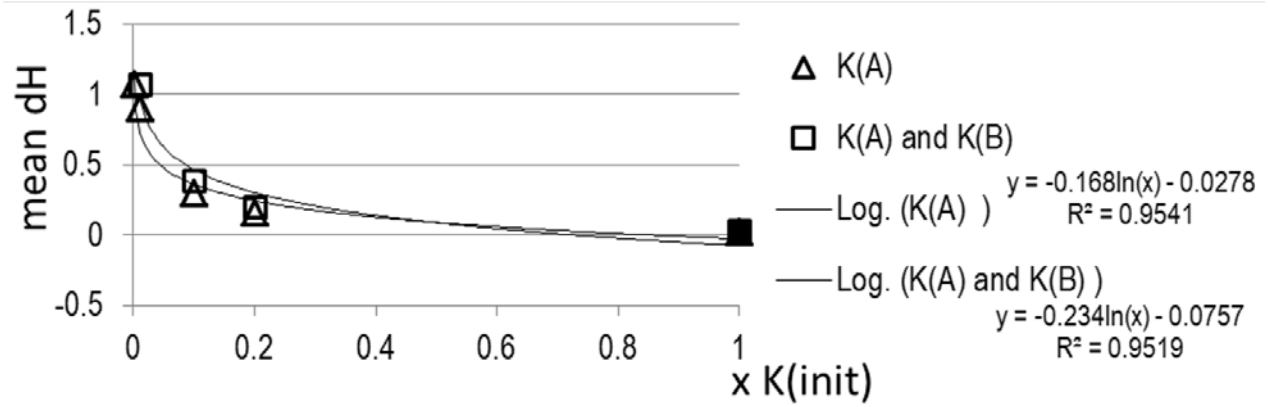

Figure A3. The effect of changing the *K* values for Layers A and B of the bog area on the water level in the selected model area (central part of the bog). dH = water level difference in m.

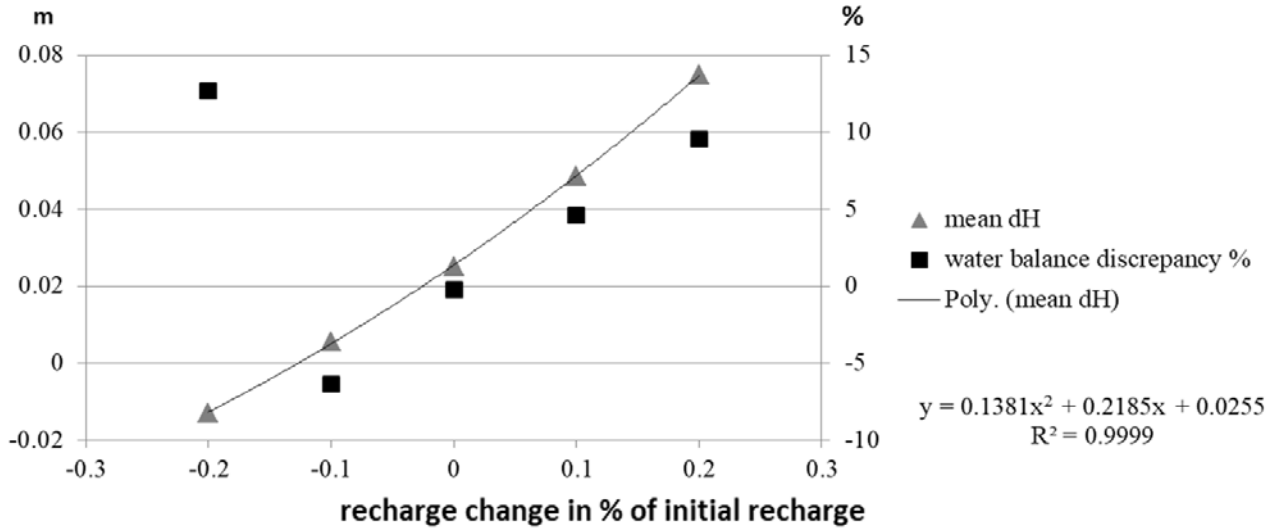

Figure A4. The effect of changing recharge to the selected model area in the central part of the bog, on the average water level ('mean dH' in m; left-hand Y-axis) and on the water balance ('water balance discrepancy' in %; right-hand Y-axis).